NASA TN D-1027

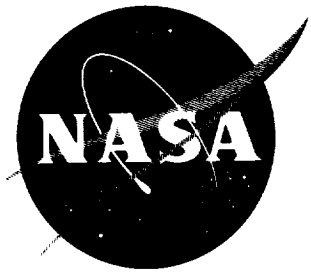

TECHNICAL NOTE

D-1027

MODEL INVESTIGATION OF THE LANDING CHARACTERISTICS OF A REENTRY SPACECRAFT WITH A VERTICAL-CYLINDER AIR BAG FOR LOAD ALLEVIATION

By John R. McGehee and Victor L. Vaughan, Jr.

Langley Research Center
Langley Air Force Base, Va.

NATIONAL AERONAUTICS AND SPACE ADMINISTRATION

WASHINGTON March 1962

NATIONAL AERONAUTICS AND SPACE ADMINISTRATION

TECHNICAL NOTE D-1027

MODEL INVESTIGATION OF THE LANDING CHARACTERISTICS OF A REENTRY SPACECRAFT WITH A VERTICAL-CYLINDER AIR BAG FOR LOAD ALLEVIATION

By John R. McGehee and Victor L. Vaughan, Jr.

SUMMARY

Analytical and experimental investigations have been made to determine the landing characteristics of a reentry spacecraft equipped with a vertical-cylinder air bag for impact load alleviation. Assuming a rigid body and isothermal air compression and expansion, computations were made to determine accelerations for a landing on concrete from a flight-path angle of 90° (vertical flight path) at a contact attitude of 0°. A scaling technique was developed which permits the application of normal scaling laws to data obtained from model tests conducted at prevailing atmospheric pressure. Two models (1/6 and 1/2 scale) of the air-bag system were tested to establish the validity of the computational procedure and the scaling technique. A 1/6-scale dynamic model of a spacecraft—air-bag configuration proposed for manned reentry was landed on concrete, on sand, and in calm water from various flight paths for a range of contact attitudes. Accelerations were measured along the X-axis (roll) and Z-axis (yaw) by accelerometers rigidly installed near the center of gravity of the model. Actual flight paths and attitudes were determined from high-speed motion pictures.

Reasonable agreement between computed and experimental data (0° attitude, 90° flight-path angle) indicates that the scaling technique is satisfactory for prediction of full-scale characteristics from model tests with air bags in atmospheric environment. The maximum accelerations obtained during landings on sand were about 11g along the X-axis and about 8g along the Z-axis. The maximum accelerations obtained during landings in water were about 10g along the X-axis and about 6g along the Z-axis. The rotational motions of the spacecraft during the time required to reach peak accelerations were small for the water and sand landings at all flight paths and attitudes of the investigation.

INTRODUCTION

The launching sites for manned reentry spacecraft are such that an aborted take-off would probably result in landing on a sandy beach or in water. These considerations have fostered a landing-load-alleviation system consisting of a vertical-cylinder air bag mounted between the reentry spacecraft and its heat shield. It is intended that the landing impact occur on the heat shield and energy be dissipated by compressing the air bag and expelling the entrapped air through orifices in the sides of the bag. Such a system might be effective in a landing on sand or in water, provided the horizontal velocity is not too great.

Analytical and experimental load-alleviation characteristics of this configuration are presented in this paper. Assuming a rigid body and isothermal air compression and expansion, computations were made to determine accelerations for a landing on concrete from a flight-path angle of 90° (vertical flight path) at a contact attitude of 0°. A scaling technique (the addition of volume for controlling compression cycle) was developed which permits the application of normal scaling laws to data obtained from model tests conducted at prevailing atmospheric pressure. The validity of the computational procedure and the scaling technique was established by comparisons with and between experimental data obtained from tests of 1/6- and 1/2-scale models. A 1/6-scale dynamic model of a spacecraft—air-bag configuration proposed for manned reentry was landed on concrete, on sand, and in calm water from various flight paths for a range of contact attitudes, and the results were extended by the scaling laws to predict the characteristics of the prototype.

SYMBOLS

A	area, sq ft
C	orifice discharge coefficient
F	force developed by air bag during landing, lb
g	acceleration due to gravity, 32.2 ft/sec^2
I	mass moment of inertia, slug-ft^2
K	volume scale factor, $\dfrac{\text{Model volume}}{\lambda^3\ (\text{full-scale volume})}$

m_c	mass of configuration, slugs
m	mass of air, slugs
p	pressure, lb/sq ft
r	radius of air bag, ft
t	time from instant of contact, sec
V	volume in air bag, cu ft
W	weight, lb
X,Y,Z	reference axes
x	air-bag stroke (measured vertically for all attitudes), ft
$\dot{x}$	velocity, ft/sec
$\ddot{x}$	acceleration, ft/sec^2
Δ	increment
λ	model scale factor, $\frac{\text{Model length}}{\text{Full-scale length}}$
ρ	density of air at standard conditions, 0.002378 slug/cu ft

Subscripts:

a	atmospheric
e	escaped
f	footprint (effective area of bag in contact with ground)
i	initial
o	orifice
t	time after contact

APPARATUS AND PROCEDURE

Three different models were tested in this investigation. Two were models (1/6 and 1/2 scale) of the air-bag system alone and were used to verify experimentally the scaling technique and computational procedure. Weights were attached to these models to simulate the weight of the reentry spacecraft. Sketches of the 1/6-scale and 1/2-scale air-bag systems are shown in figure 1. The third model was a 1/6-scale dynamic model of the reentry spacecraft complete with air-bag system and this model was used to investigate the landing behavior of the full-scale system. A sketch of the 1/6-scale dynamic model is shown in figure 2. Figures 3 and 4, respectively, are photographs of the 1/6-scale dynamic model and a 1/6-scale geometric model of the full-scale configuration. Sketches identifying axes, flight paths, and contact attitudes are shown in figure 5. Dimensions and velocities for the 1/6-scale and the 1/2-scale air-bag models are presented in table I. Pertinent values for the 1/6-scale dynamic model and the full-scale configuration are presented in table II.

L 1 3 -1 9

Scaling

The scaling laws employed in the testing of dynamic models (models with scaled mass and mass moments of inertia) require pressure to be scaled directly as the scale factor. If these scaling laws were rigorously followed, model testing (when air compression is involved) would have to be conducted in a controlled atmosphere. To avoid this complication, a method of scaling which permits the testing of these dynamic models at prevailing atmospheric conditions has been developed.

If the volume of the air bag of a dynamic-model—air-bag configuration were scaled and the atmospheric pressure were not scaled, the pressure rise during compression would be greater in the model than in the prototype. Therefore, it is necessary to alter the compression cycle in the model to approximate the compression cycle that would occur with the full-scale configuration. One method of controlling the compression cycle is by increasing the initial volume of gas involved. This change in volume must be made without changing the geometric shape of the air bag in order that the forces and motions obtained will be scaled values of the forces and motions of the full-scale configuration. In this investigation the additional volume required was obtained by replacing the upper part of the model with an air compartment having the desired volume. A computational procedure, which is presented in this paper, was employed to compute acceleration time histories for the full-scale configuration and for various models of differing scales with corresponding additional volumes. The volume scale factor K was

determined by dividing the volume required to match computed model and full-scale acceleration time histories by the product of the cube of the scale factor λ and the full-scale volume. The additional volume required, as indicated by these computations, was incorporated in the 1/6-scale air-bag model by adding the air compartment mentioned previously. The validity of this method of approximating the compression cycle, and hence the acceleration time histories of the full-scale configuration, was checked by testing the 1/6-scale and 1/2-scale air-bag models. It should be emphasized that this method of scaling the compression cycle results in only an approximation of the acceleration time histories of the full-scale configuration. The scale factors for the various parameters were determined by using this procedure and are shown in table III.

Description of Models

The 1/6-scale and 1/2-scale air-bag models were constructed of 3/4-inch plywood disks and 0.010-inch balloon cloth. Two layers of balloon cloth were required to prevent bursting of the 1/2-scale air-bag model. Sixty-four orifices of 3/4-inch diameter were used in the 1/2-scale model and were drilled through the upper disk.

The 1/6-scale air-bag model had a sealed, aluminum air compartment mounted above the upper plywood disk and this air compartment was open to the air bag. The total area of the openings between the air compartment and air bag was approximately 3 times greater than the total orifice area of the air bag, permitting the orifice area to control the pressure rise of the air-bag—air-compartment combination. Seven orifices of 3/4-inch diameter were cut in the air bag. The cloth in the vicinity of the orifices was reinforced to prevent this weakened section from collapsing and reducing the orifice area. The required ballast weights were rigidly attached in the center of the upper disks of both models.

The 1/6-scale dynamic model (model with scaled mass and mass moments of inertia) was constructed of fiber glass and plastic and the construction was as stiff as possible to reduce structural vibrations. The air compartment was spherical in shape in order to obtain maximum strength, maximum structural rigidity, and maximum volume for the lightest weight. The mass moments of inertia were kept as low as possible but, because of the addition of the spherical air compartment, the desired scale values could not be obtained. (See table II.) The vertical-cylinder air bag was made of 0.010-inch balloon cloth and was attached between the model and the heat shield. The 3/4-inch orifices were cut in the balloon cloth and the cloth in the vicinity of the seven orifices was reinforced to prevent this weakened section from being the first to collapse on impact and thus closing the orifices.

Instrumentation

The instrumentation for the model tests consisted of single-component accelerometers, a 3-kc amplifier, and a recording oscillograph. The accelerometers were capable of measuring 50g, their natural frequency was about 600 cps, and they were damped to about 80 percent of critical damping. The response of the recording equipment was flat to about 600 cps. One accelerometer, alined along the X-axis of the air bag, was used in the air-bag scaling investigation; two accelerometers, alined along the X-axis and Z-axis, respectively, were used for the dynamic-model test. The accelerometers were rigidly attached to the upper disk of the air-bag models. In the dynamic-model test they were attached near the center of gravity of the configuration.

L
1
3
1
9

Test Methods

Tests for a 90° flight-path angle, which simulates a parachute letdown with no wind velocity, were made by a free-fall method where the model was dropped from the height required to obtain, under the influence of gravitational acceleration, a vertical velocity at contact equivalent to 30 fps full scale. Tests for nominal 60° and 27° flight-path angles, which simulate, respectively, parachute letdowns with horizontal wind velocities of about 17 and 59 fps (full scale) were conducted by releasing the model from a pendulum and allowing it to free fall to the landing surface. This test procedure is discussed in detail in reference 1. A range of contact attitudes from -28° to 30° was used for all flight paths in the investigation. This range simulated contact attitudes that might occur due to parachute oscillation. The contact attitudes, flight paths, and motions were recorded by a high-speed motion-picture camera. The air-bag landings for the scaling investigation were made on a smooth concrete floor. The landings of the dynamic model were made on concrete, on dry Ottawa testing sand, and in water.

Computations

Acceleration time histories were computed for models landing on a vertical-cylinder air bag from a vertical flight path at a 0° contact attitude. The equations employed in these computations are as follows:

$$F = m_c\ddot{x} = m_c \frac{d^2x}{dt^2} = m_c \frac{d\dot{x}}{dt} = m_c \frac{\Delta\dot{x}}{\Delta t}$$

The decelerating force at any time after contact is equal to the product of the footprint area of the bag and the gage pressure in the bag

$$F_t = A_{f,t} p_{t,gage}$$

The footprint area of the air bag at any time after contact $A_{f,t}$ is

$$A_{f,t} = \pi r^2$$

The gage pressure in the air bag at any time after contact $p_{t,gage}$ may be determined from the pressure-volume relation. When isothermal compression and expansion are assumed

$$p_{t,gage} = \frac{p_i V_i}{V_t} \frac{m_i - m_{e,t}}{m_i} - p_a$$

where $m_{e,t}$ is the mass of air escaping through the orifices.

The volume of air in the bag at any time after contact may be computed from the following equation:

$$V_t = V_i - \sum A_{f,t} \Delta x$$

where $\sum A_{f,t} \Delta x$ represents the volume change due to compression.

The mass of air that has escaped $m_{e,t}$ may be determined from the following equation:

$$m_{e,t} = \sum \Delta m_{e,t} = \sum \rho_t C A_o \Delta t \sqrt{\frac{2p_a}{\rho_t}\left(\frac{p_{t-\Delta t}}{p_a} - 1\right)}$$

This equation is valid as long as the absolute pressure in the air bag is less than $1.9p_a$. For values of $p_t \geqq 1.9p_a$ the velocity of air through the orifices is the acoustic velocity.

The decelerating force at any time after contact may now be rewritten in the following form:

$$F_t = \pi r^2 \left[\left(\frac{p_i V_i}{V_t} \frac{m_i - m_{e,t}}{m_i} \right) - p_a \right]$$

With these equations, acceleration time histories were calculated by using a step-by-step procedure which employs the transformation $\frac{d^2x}{dt^2} = \frac{d\dot{x}}{dt} = \frac{\Delta\dot{x}}{\Delta t}$ and where each step is defined by a small increment of the independent variable time Δt. For the purpose of these computations, the following assumptions were made: (1) parachute release occurred at contact and the only force causing deceleration was the gas-pressure force, (2) the air-bag material was inextensible and collapsible, and (3) the orifice discharge coefficient was 0.8.

L 1 3 1 9

RESULTS AND DISCUSSION

Scaling Technique

The volume scale factor K, as determined from computations, is shown plotted as a function of model scale factor λ in figure 6. These factors are applicable for the full-scale configuration weight, velocity, and pressure presented in this paper and it is recommended that the suitability of these factors be established when parameters radically different from those of the present investigation are considered.

The correlation between acceleration time histories obtained from the 1/6-scale and 1/2-scale air-bag models for landings on concrete from a vertical flight path at 0° contact attitude and computed acceleration time histories for these air-bag models are shown in figure 7. Good agreement was obtained between the experimental and computed data for both the 1/6-scale and 1/2-scale air bags.

For purposes of establishing the validity of the scaling technique, the 1/6-scale air-bag data were scaled to 1/2 scale by employing the scaling factors shown in table III. A volume scale factor of 2.5 was determined from figure 6 by using the applicable model scale factor of $\frac{1/6}{1/2} = \frac{1}{3}$. This procedure resulted in good agreement between the data. (See fig. 7.)

Dynamic-Model Investigation

Experimental data obtained from the 1/6-scale dynamic model for a landing on concrete from a vertical flight path at a 0° contact attitude and computed data for the full-scale configuration are shown in figure 8. The volume scale factor for the 1/6-scale dynamic model was determined from figure 6 to be 5.0. Computed full-scale-configuration data and data obtained by scaling results from the 1/6-scale dynamic-model tests were in reasonable agreement. Sequence photographs of the 1/6-scale dynamic model landing on concrete are shown in figure 9.

The distorted geometry of the upper portion of the model destroys similarity between the model and the full-scale configuration when the sphere comes into contact with the landing surface. Therefore, the minimum time for each flight path at which the sphere contacts the landing surface is indicated on the pertinent figures in the following discussion.

Sand landings.- Typical time histories of accelerations along the X-axis and Z-axis obtained in landings of the dynamic model on sand are shown in figures 10 and 11, respectively, for landings from 90° and 62° flight-path angles at various contact attitudes. In all cases the maximum acceleration occurred before the sphere contacted the landing surface. The small initial negative accelerations shown on figure 10(a) for the 28° contact attitude and on figure 10(b) for the 30° and -28° contact attitudes may be attributed to a tension force which is developed in the air-bag material when the heat shield impacts the sand unsymmetrically.

Maximum accelerations for landings made on sand are shown for the X-axis and Z-axis as a function of contact attitude, with flight-path angle as a parameter, in figure 12. The maximum acceleration along the X-axis for the 90° flight-path angle was approximately 11g and occurred at a contact attitude of 0°. For the 62° flight-path angle, the maximum acceleration along the X-axis was about 10g and occurred at a contact attitude of 30°. The maximum acceleration along the Z-axis was about 8g and occurred at a contact attitude of -28°. It should be noted that greater accelerations along the Z-axis would probably have been encountered for each flight path if more extreme contact attitudes had been investigated.

Water landings.- Typical acceleration time histories for accelerations along the X-axis for landings in water are shown in figure 13 for flight-path angles of 90°, 60°, and 27° at various contact attitudes. The small initial negative acceleration, shown at the positive contact attitude, is believed to have resulted from tension in the leading edge of the air bag. Shortly after contact the gas-compression force in the

air bag became the dominant force and the acceleration became positive. In all cases the maximum acceleration occurred before the sphere contacted the water.

The abrupt increase in acceleration shown for the 27° flight-path angle at the -21° contact attitude is believed to have been caused by the heat shield impacting the bottom of the model. This is a result of the relatively high horizontal velocity associated with this flight path. The values of acceleration shown for the impact between the heat shield and the model should not be used quantitatively because of the limited response of the instrumentation.

Typical time histories of accelerations along the Z-axis are shown in figure 14 for landings in water from flight-path angles of 90°, 60°, and 27° at various contact attitudes. As was the case for the acceleration along the X-axis, the abrupt rise in acceleration shown for the 27° flight-path angle and a -21° contact attitude was likely caused by the heat shield impacting the bottom of the model.

Maximum accelerations along both the X-axis and Z-axis during water landings are plotted in figure 15 as a function of contact attitude with flight-path angle as a parameter. The maximum accelerations along the X-axis, for both the 90° and 62° flight-path angles, were between 6g and 7g and changed little with variation in contact attitude. For the 27° flight-path angle, the maximum acceleration along the X-axis was approximately 10g and occurred at a contact attitude of 0°. Increasing the contact attitude in either the positive or negative direction for the 27° flight-path angle resulted in a decrease of the magnitude of the maximum acceleration. The maximum acceleration along the Z-axis obtained in the test occurred at a flight-path angle of 27° and a contact attitude of approximately -21° and was about 6g. It should be noted that greater accelerations along the Z-axis would probably have been encountered for each flight path if more extreme contact attitudes had been investigated.

Angular motions.- Attitude time histories for landings in sand and water are presented in figures 16 and 17, respectively, for the range of flight paths and contact attitudes of the investigation. In general, the rate of rotation of the model during the time required to reach peak acceleration was small for all flight paths and contact attitudes. The spherical upper portion of the model did not contact the landing surface during the time periods shown in figures 16 and 17.

CONCLUDING REMARKS

The landing characteristics of a 1/6-scale model of a reentry spacecraft equipped with a vertical-cylinder air bag for load alleviation

were determined by analytical and experimental investigations. It was found that there was good agreement between computed and experimental data obtained from landings on concrete from a 90° flight-path angle (vertical flight path) at 0° contact attitude. The scaling technique, which was developed to permit the application of the scaling laws for dynamic-model testing to data obtained from model tests conducted at prevailing atmospheric conditions, appeared to be satisfactory for predicting the landing accelerations for the full-scale configuration. The maximum accelerations obtained for sand landings were about 11g along the X-axis (roll) and about 8g along the Z-axis (yaw). The maximum accelerations obtained for smooth water landings were about 10g along the X-axis and about 6g along the Z-axis. The rotational motions of the model, during the time required to reach peak acceleration, were small for all flight paths and contact attitudes investigated in landings on sand or water.

Langley Research Center,
National Aeronautics and Space Administration,
Langley Air Force Base, Va., December 13, 1961.

REFERENCE

1. McGehee, John R., Hathaway, Melvin E., and Vaughan, Victor L., Jr.: Water-Landing Characteristics of a Reentry Capsule. NASA MEMO 5-23-59L, 1959.

TABLE I.- PERTINENT DIMENSIONS AND VELOCITIES FOR

1/6-SCALE AND 1/2-SCALE AIR-BAG MODELS

	1/6 scale	1/2 scale
Weight of configuration, lb	10.2	258
Simulated weight of heat shield, lb	1.2	15
Height of air bag, ft	0.67	2.00
Diameter of air bag, ft	1.03	3.1
Footprint area, sq ft	0.83	7.48
Volume of air bag, cu ft	1.385	14.96
Total area of orifices, sq ft	0.022	0.197
Velocity at contact, fps	12.25	21.20

TABLE II.- PERTINENT VALUES FOR 1/6-SCALE DYNAMIC MODEL

AND FULL-SCALE CONFIGURATION

	1/6 scale (measured values)	Full-scale configuration
Weight of configuration, lb	10.56	2,260
Weight of heat shield, lb	1.45	314
Location of center of gravity above upper edge of bag, ft	0.263	1.58
I_X (roll), slug-ft^2	0.060	------
I_Y (pitch), slug-ft^2	0.121	276
I_Z (yaw), slug-ft^2	0.121	276
Diameter of air bag, ft	1.03	6.20
Total area of orifices, sq ft	0.022	0.77
Initial volume of air bag, cu ft	2.80	121.10
Velocity at contact, fps	12.25	30.00
Height of air bag, ft	0.67	4.00

TABLE III.- SCALING FACTORS

L
1
3
1
9

Quantity	Full scale	Scale factor	Model
Area	A	λ^2	$\lambda^2 A$
Force	F	λ^3	$\lambda^3 F$
Mass	m_c	λ^3	$\lambda^3 m_c$
Length	x	λ	λx
Volume	V	$K\lambda^3$	$K\lambda^3 V$
Weight	W	λ^3	$\lambda^3 W$
Velocity	$\dot{x}$	$\lambda^{0.5}$	$\lambda^{0.5}\dot{x}$
Acceleration	$\ddot{x}$	≈ 1	$\approx \ddot{x}$
Air-bag pressure (gage). .	p	$\approx\lambda$	$\approx\lambda p$
Ambient pressure	p_a	1	p_a
Time	t	$\lambda^{0.5}$	$\lambda^{0.5} t$
Inertia	I	λ^5	$\lambda^5 I$

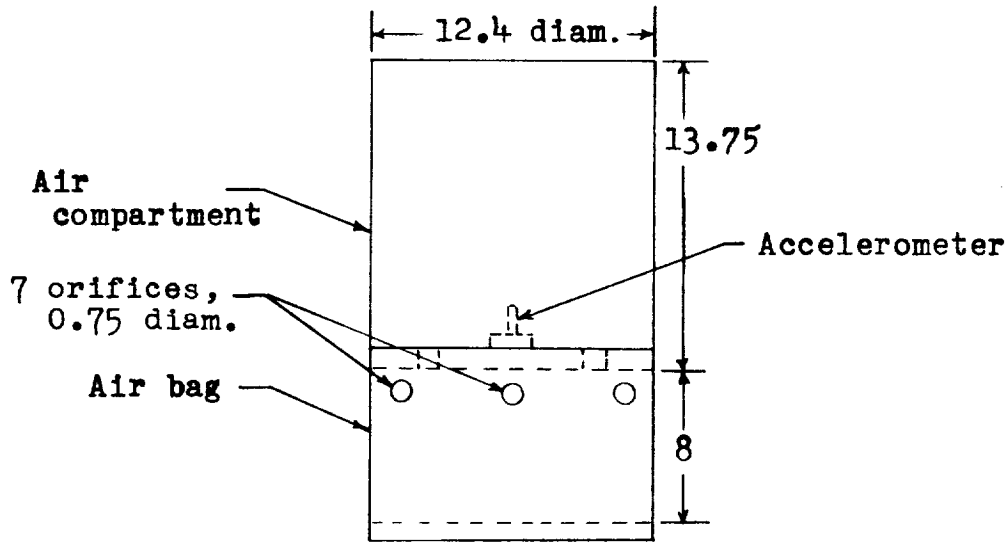

(a) 1/6-scale air-bag model.

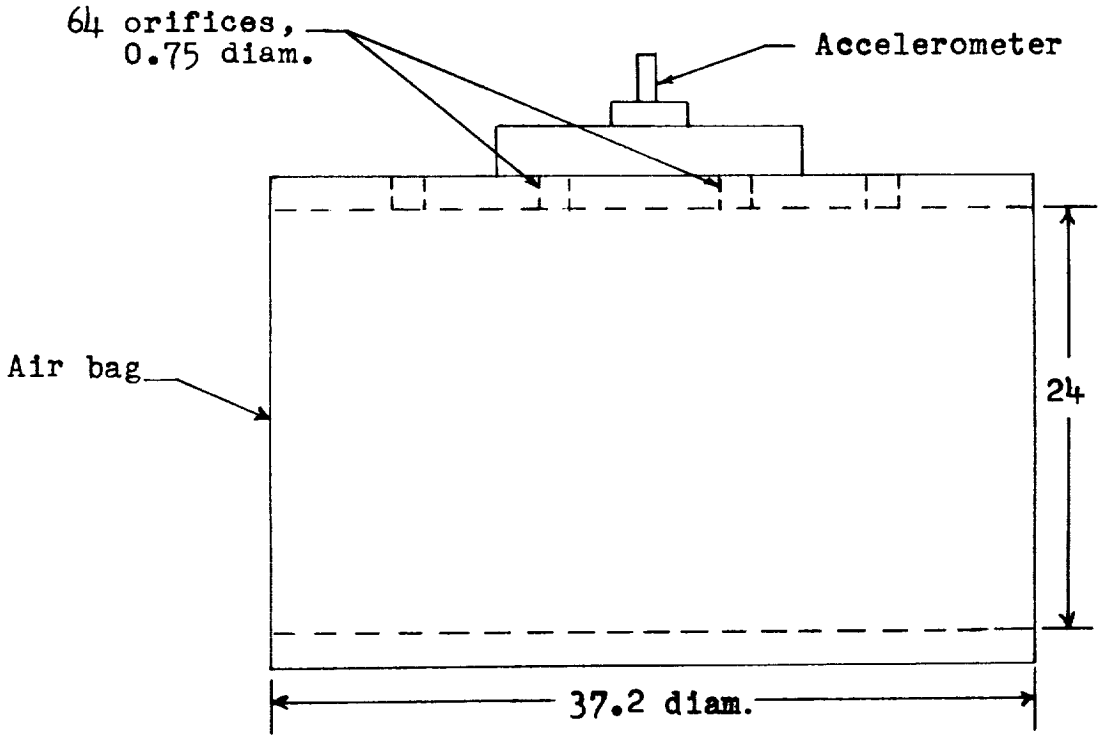

(b) 1/2-scale air-bag model.

Figure 1.- Air-bag models used in scaling investigation. All dimensions are in inches.

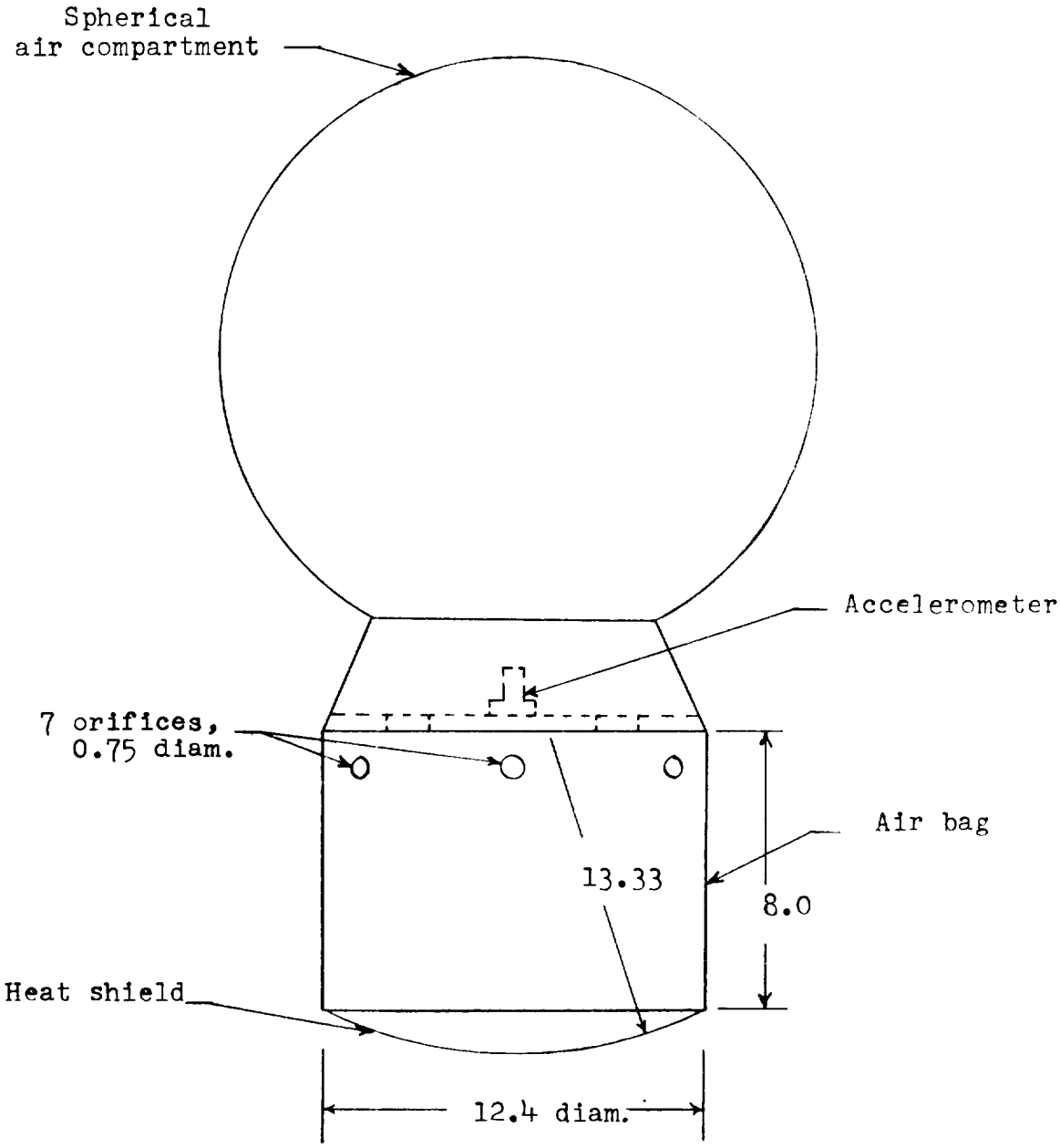

Figure 2.- 1/6-scale dynamic-model configuration. All dimensions are in inches.

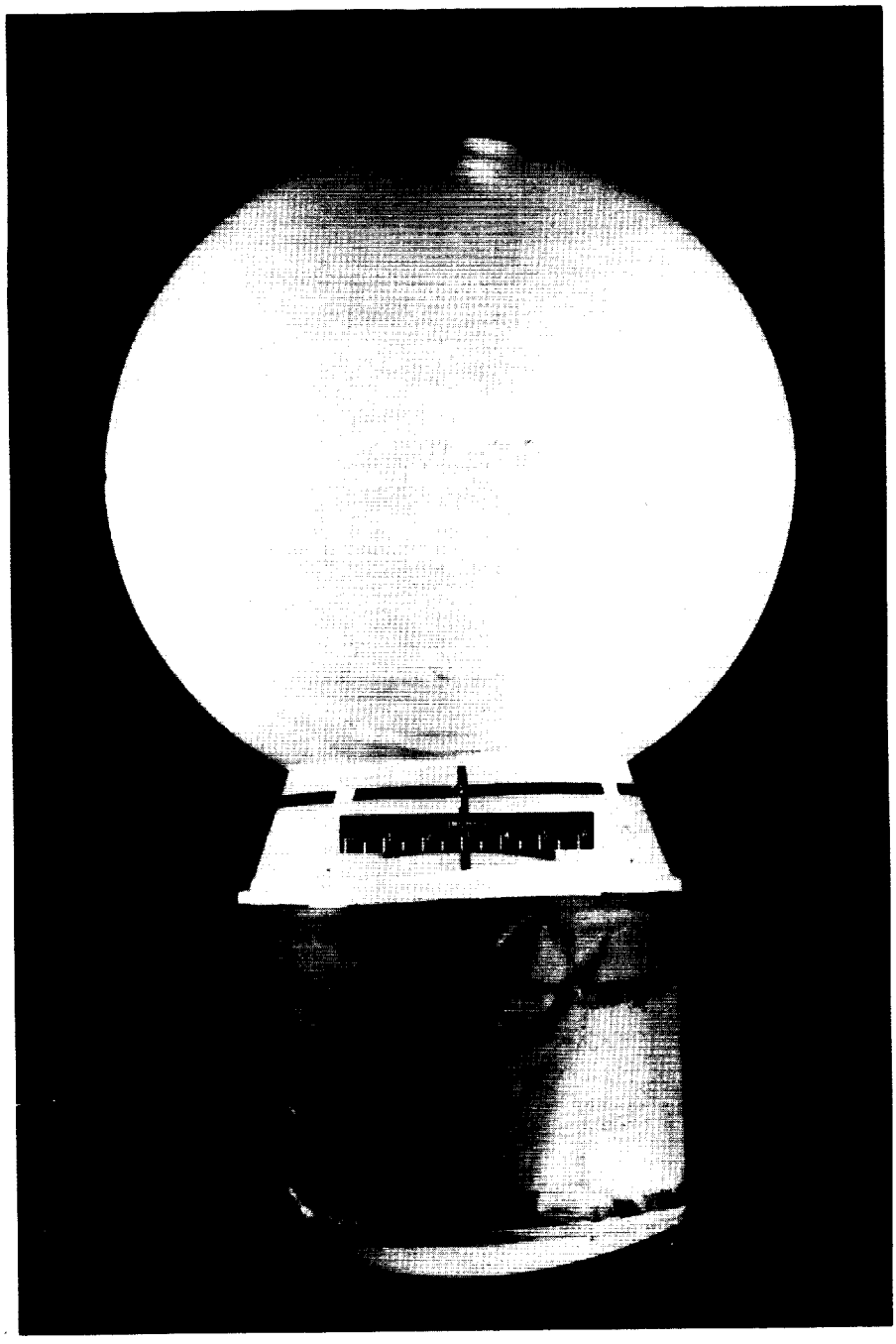

L-60-2652

Figure 3.- Photograph of 1/6-scale dynamic-model configuration.

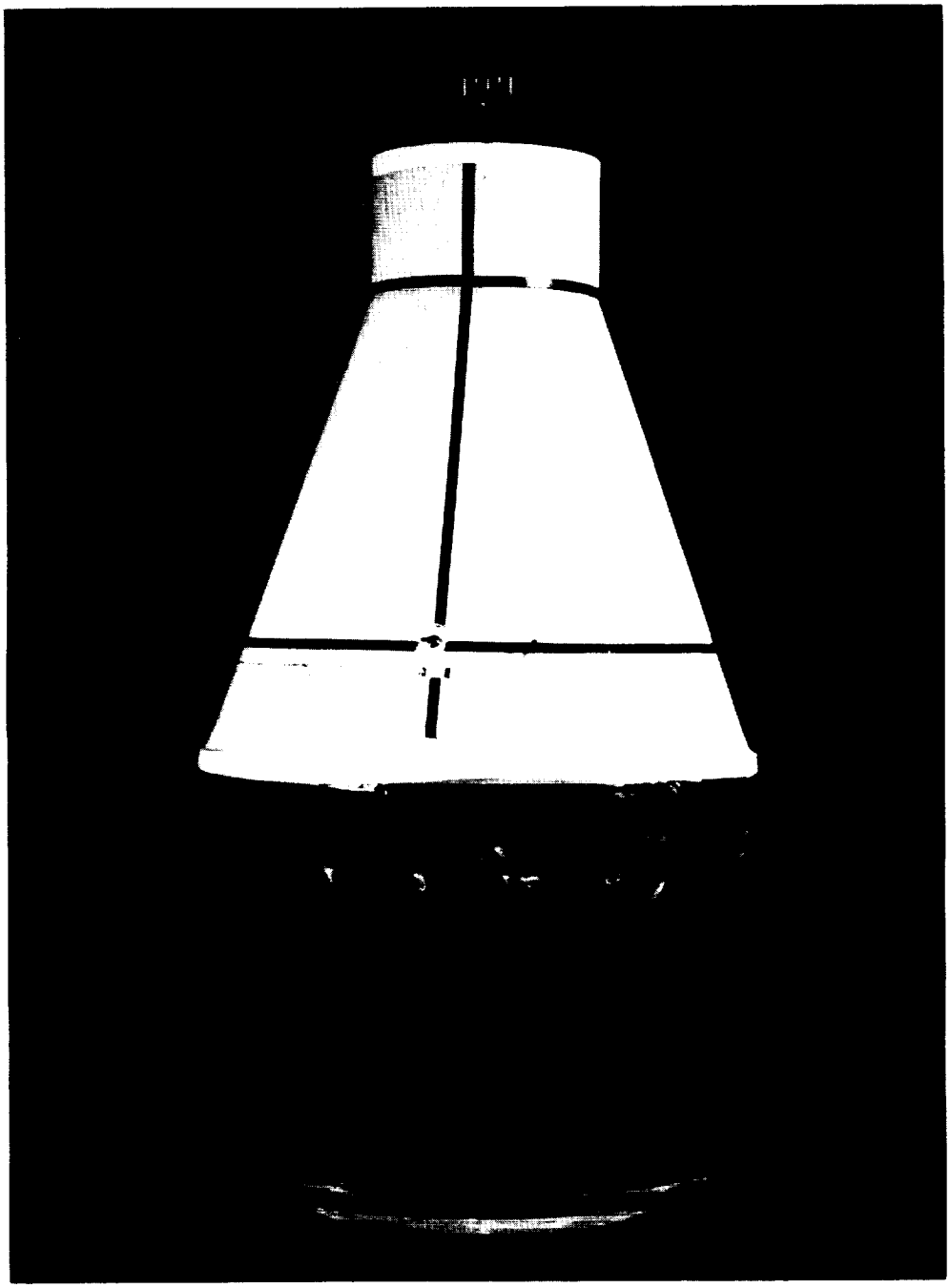

L-60-1281

Figure 4.- Photograph of 1/6-scale geometric model of full-scale configuration.

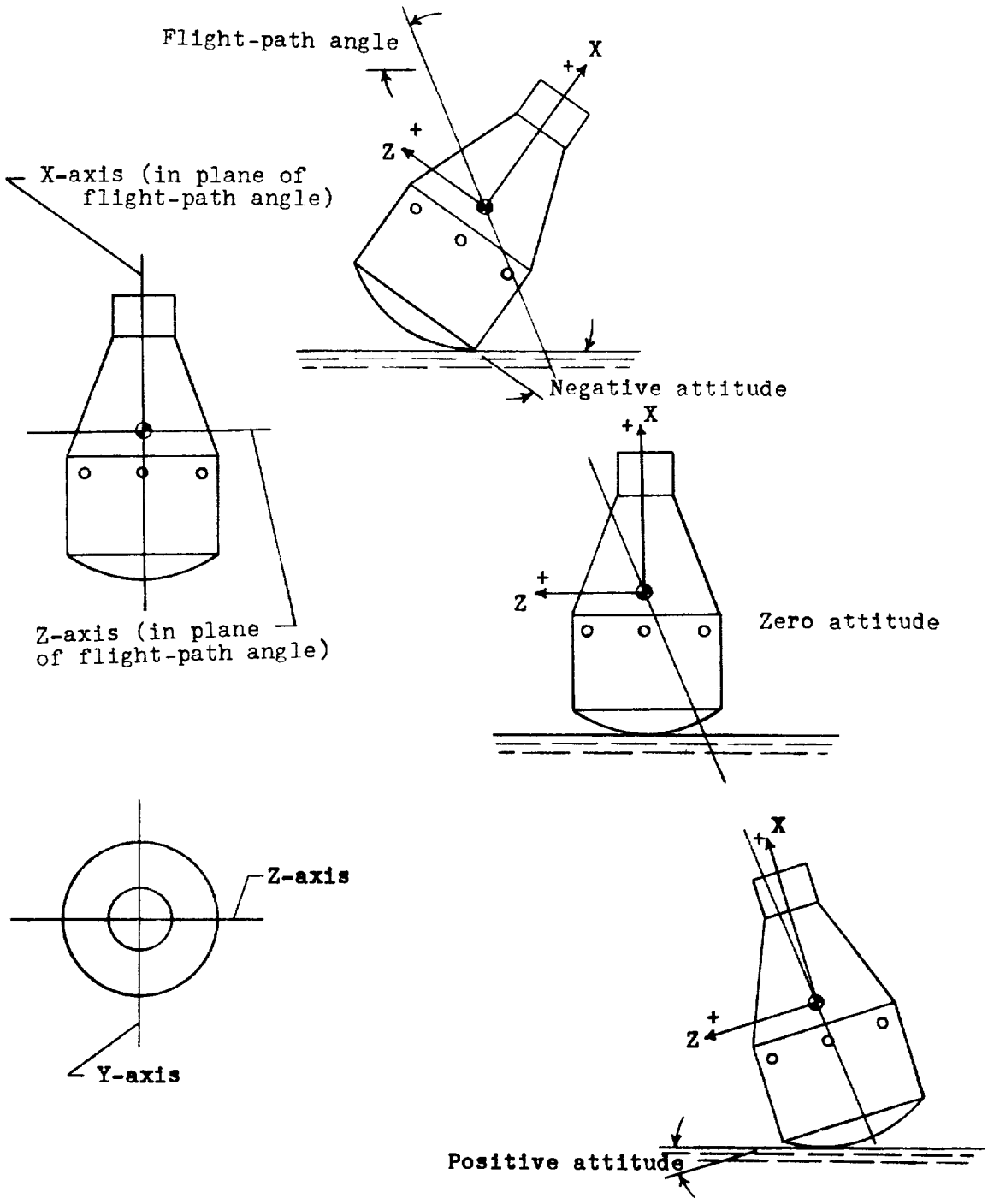

Figure 5.- Sketches identifying axes, flight paths, and contact attitudes.

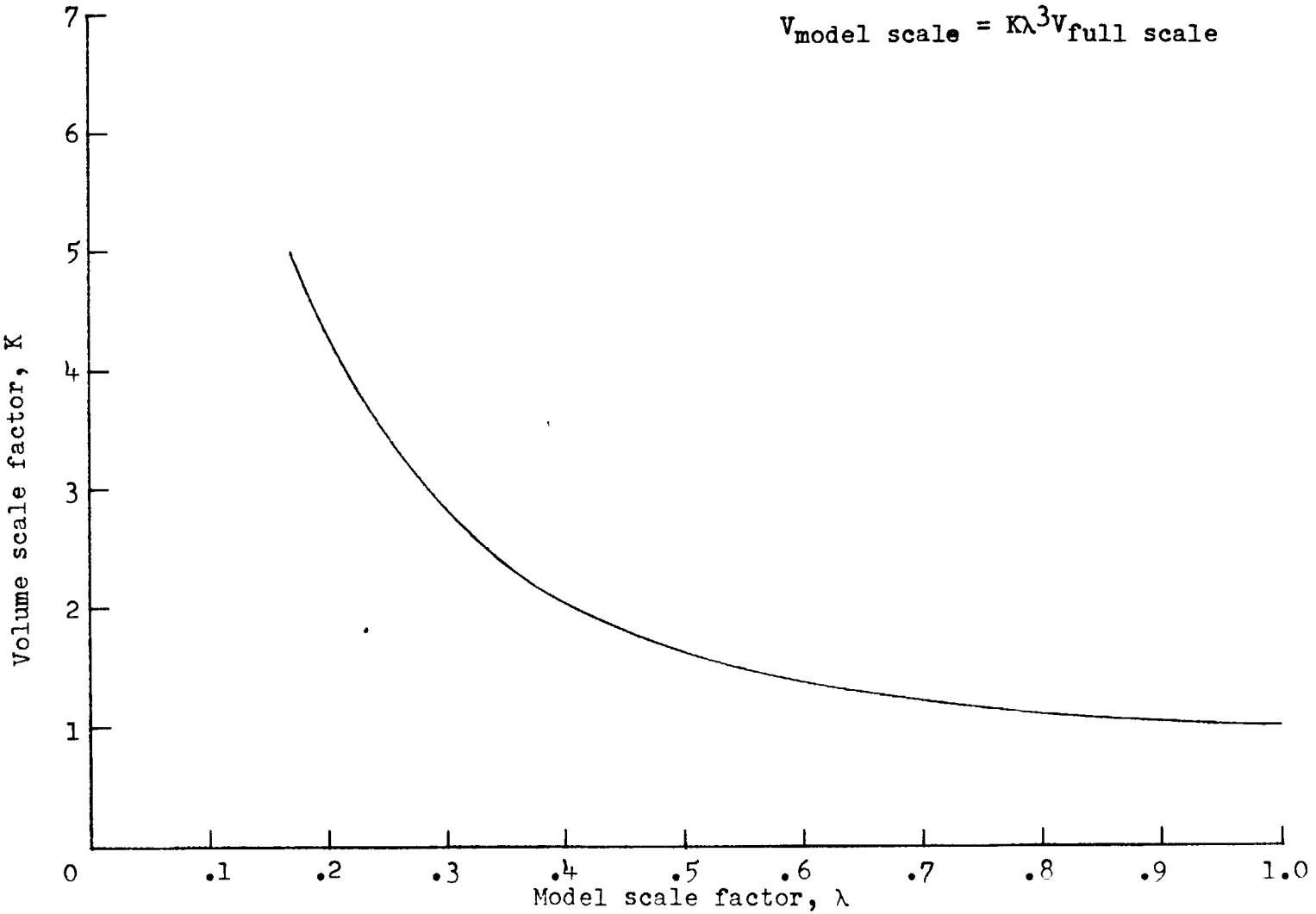

Figure 6.- Computed volume scale factor as a function of model scale factor.

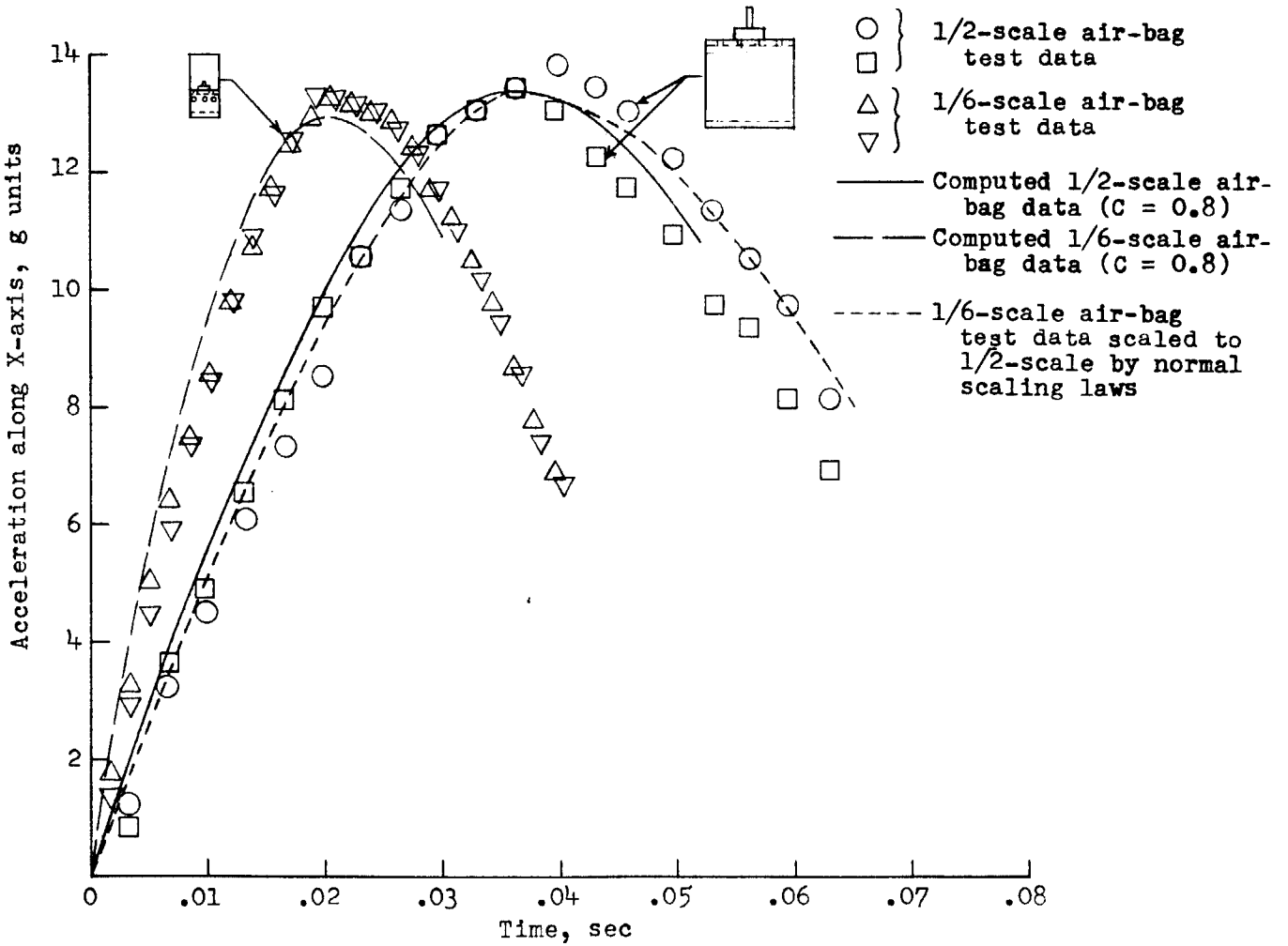

Figure 7.- Correlation between experimental and computed acceleration time histories obtained from 1/6-scale and 1/2-scale air-bag tests. Vertical flight path; 0° contact attitude; landing on concrete.

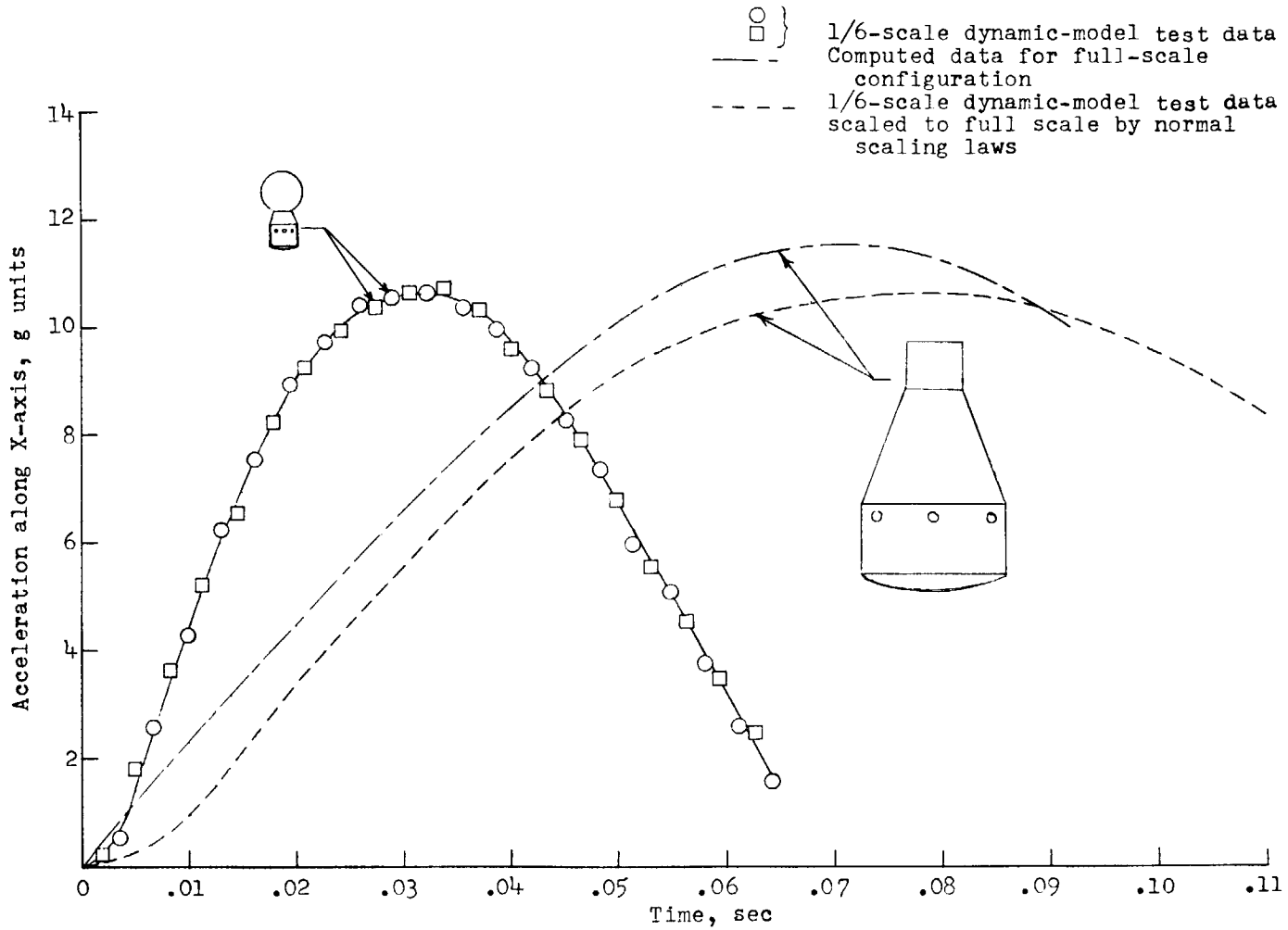

Figure 8.- Correlation between acceleration time histories of 1/6-scale dynamic-model test and computed data for full-scale configuration. Vertical flight path; 0° contact attitude; landing on concrete.

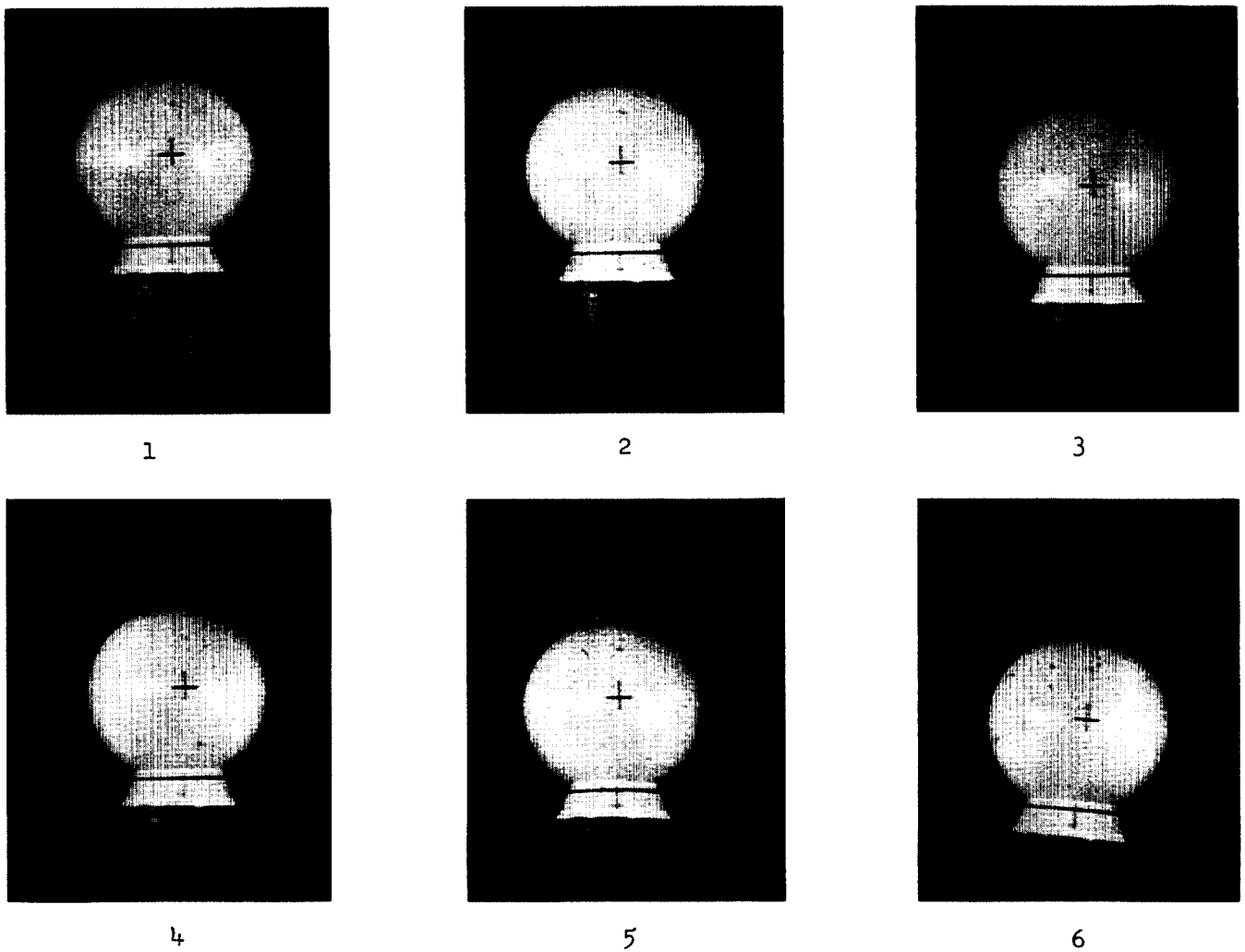

L-61-8414

Figure 9.- Sequence photographs for landing on concrete from vertical flight path at 0° contact attitude.

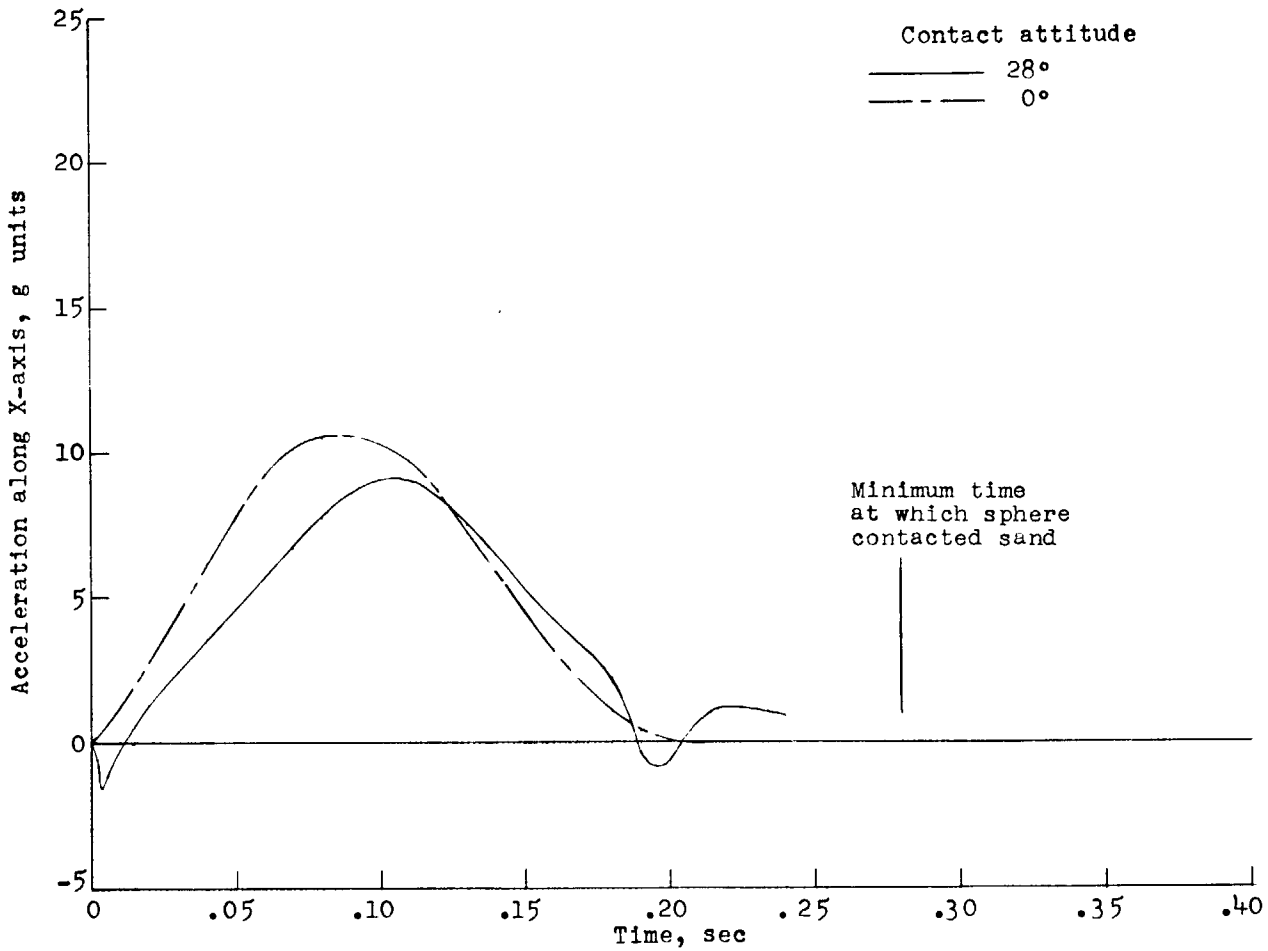

(a) Flight-path angle, 90°.

Figure 10.- Typical acceleration time histories along X-axis for landings on sand. All values are full scale.

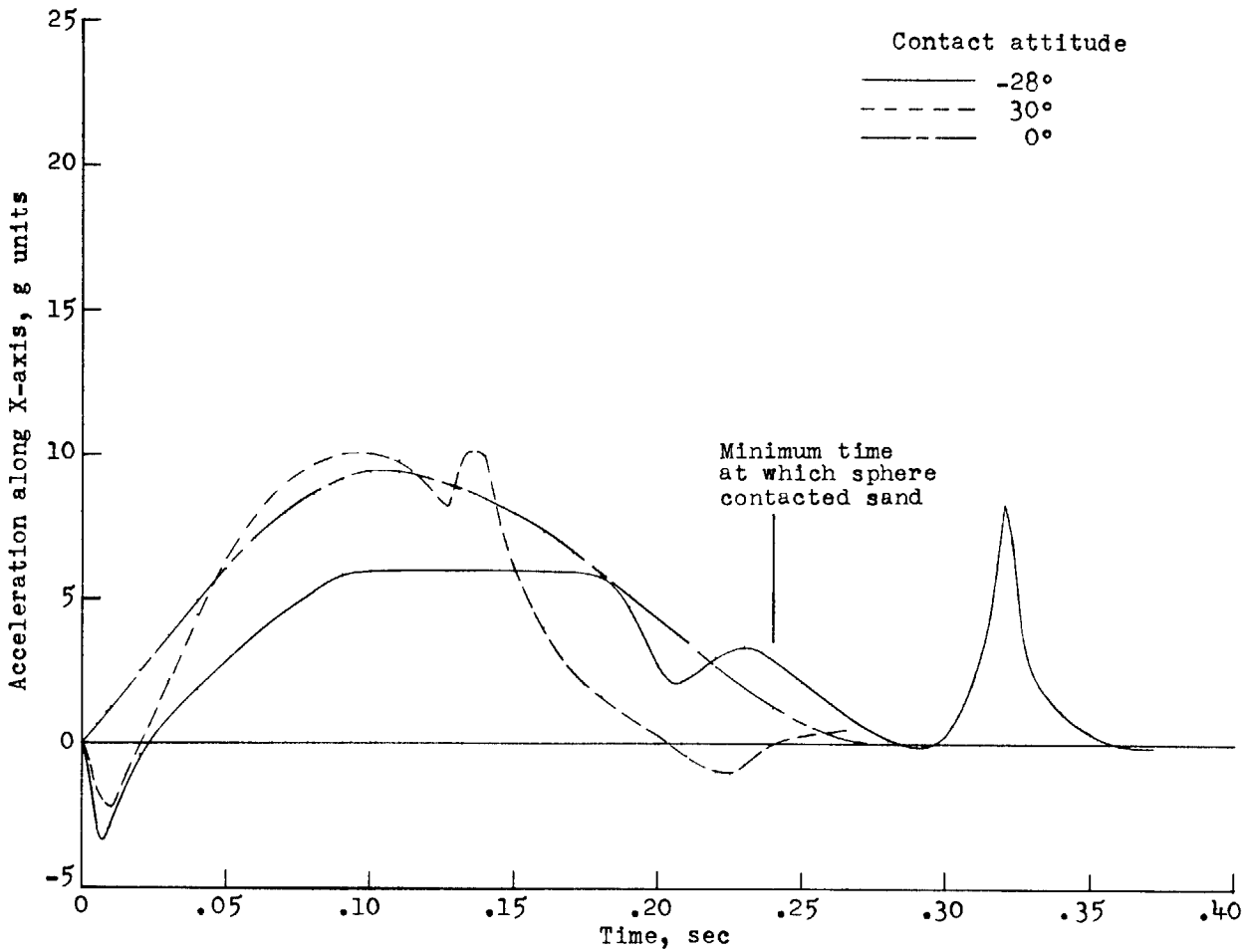

(b) Flight-path angle, 62°.

Figure 10.- Concluded.

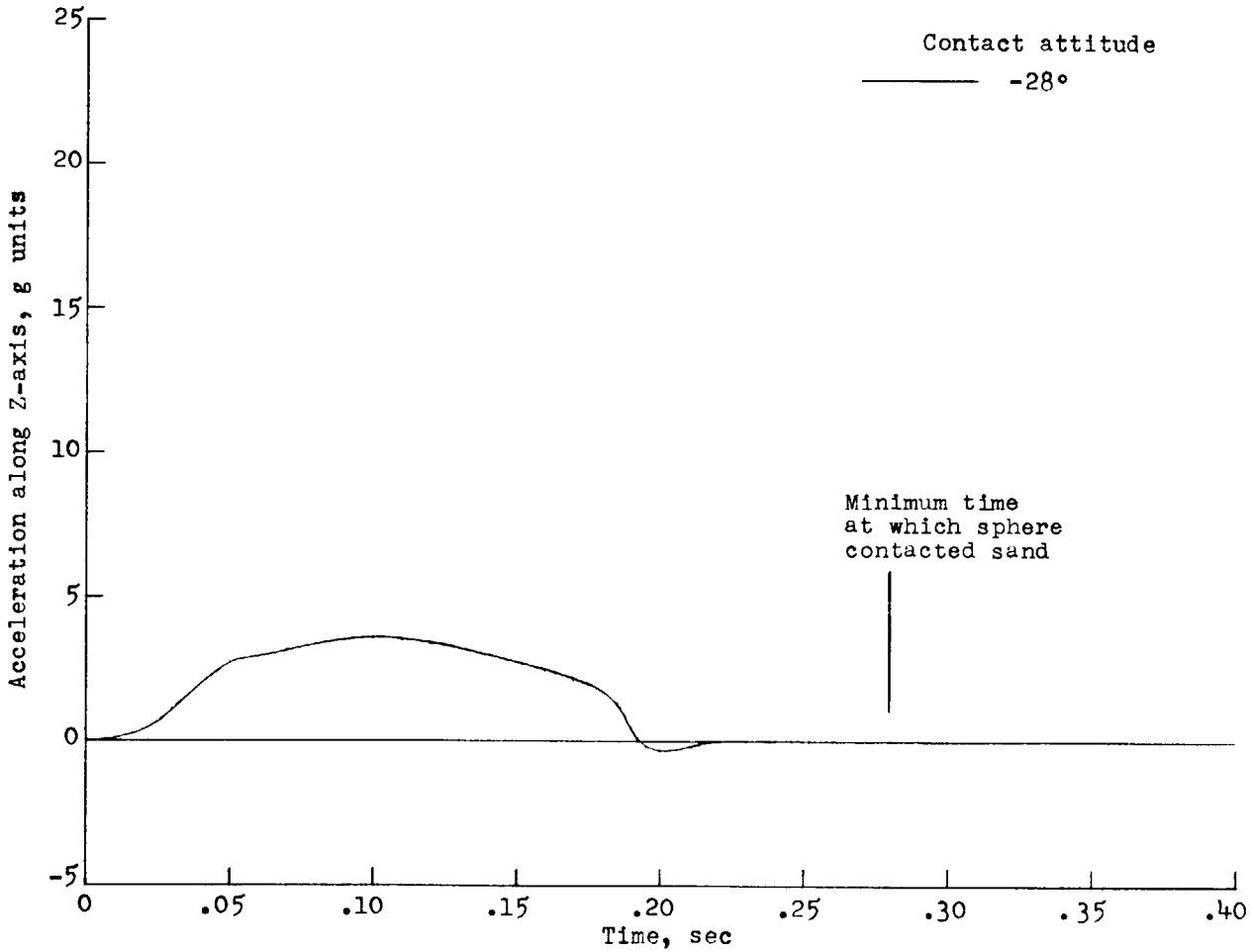

(a) Flight-path angle, 90°.

Figure 11.- Typical acceleration time histories along Z-axis for landings on sand. All values are full scale.

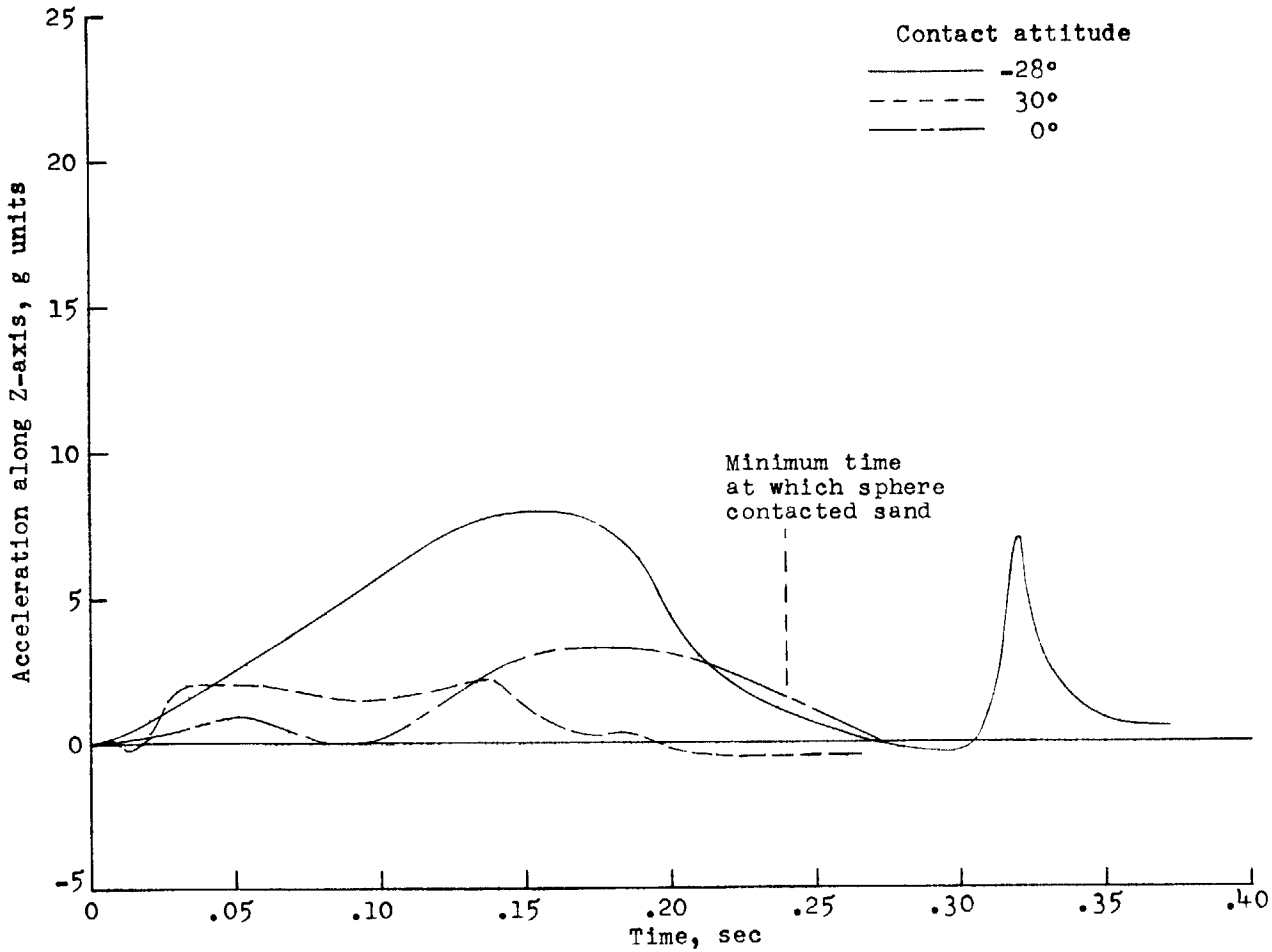

(b) Flight-path angle, 62°.

Figure 11.- Concluded.

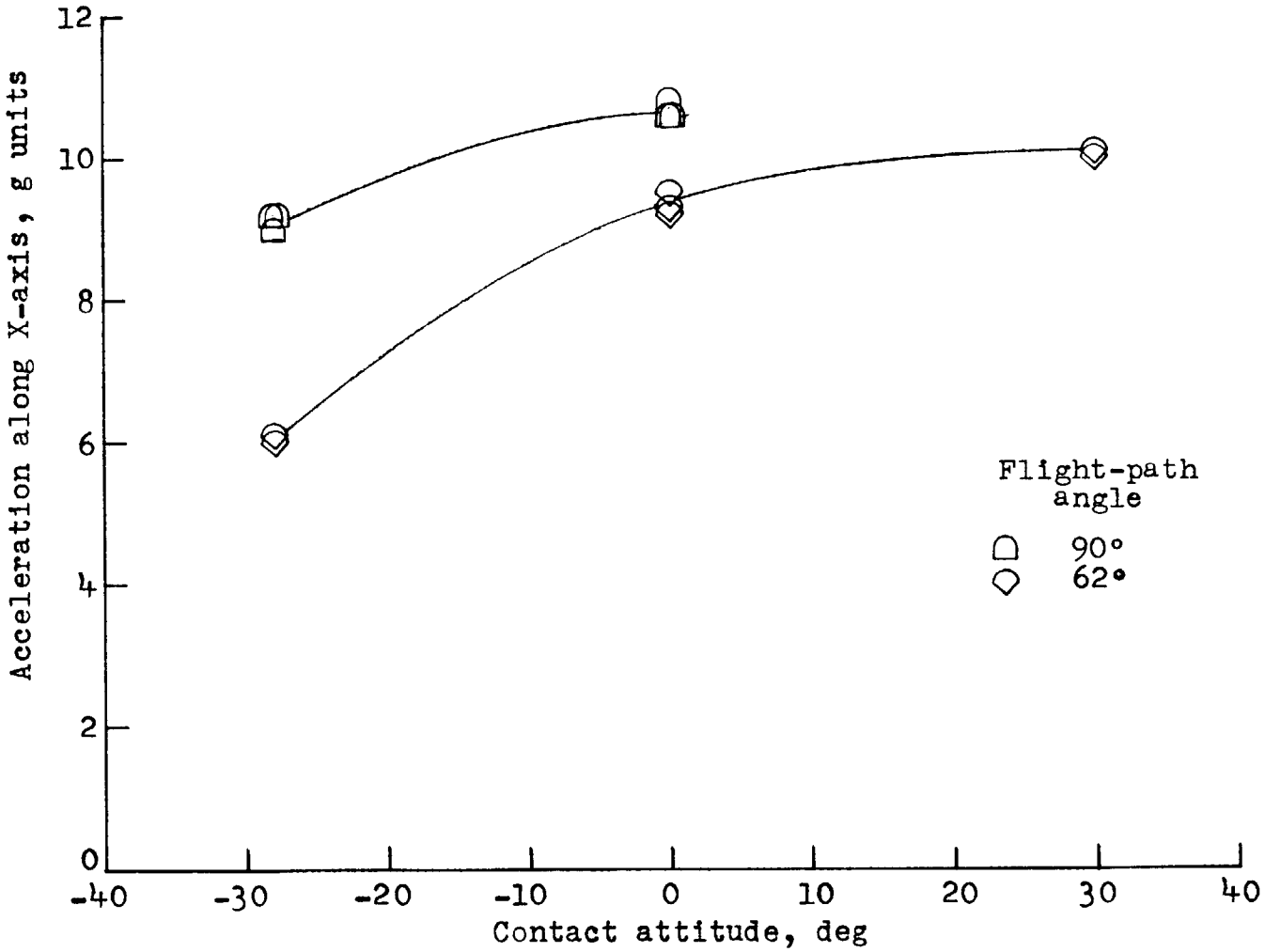

(a) X-axis.

Figure 12.- Maximum accelerations for landings on sand.

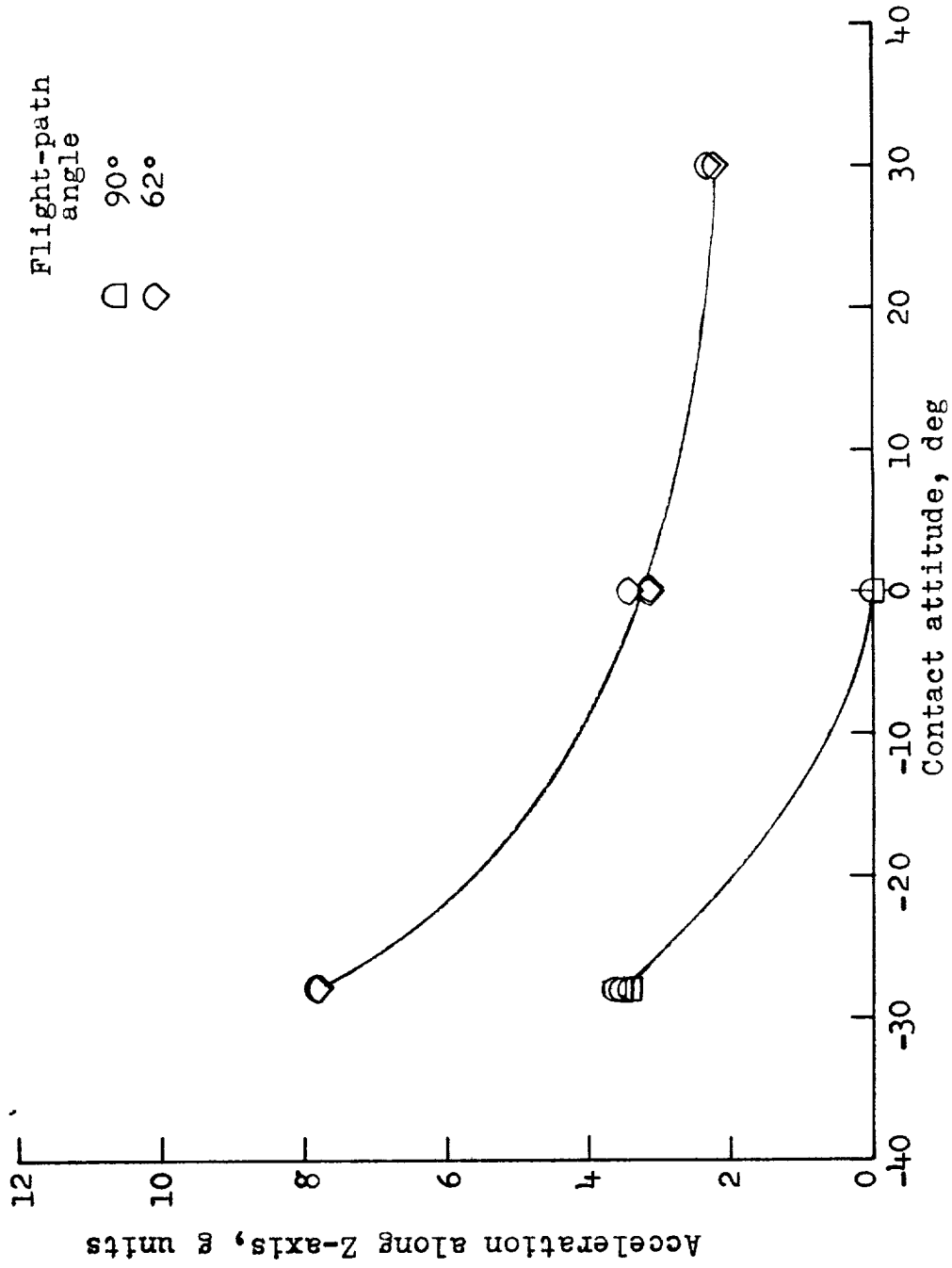

(b) Z-axis.

Figure 12.- Concluded.

L-1519

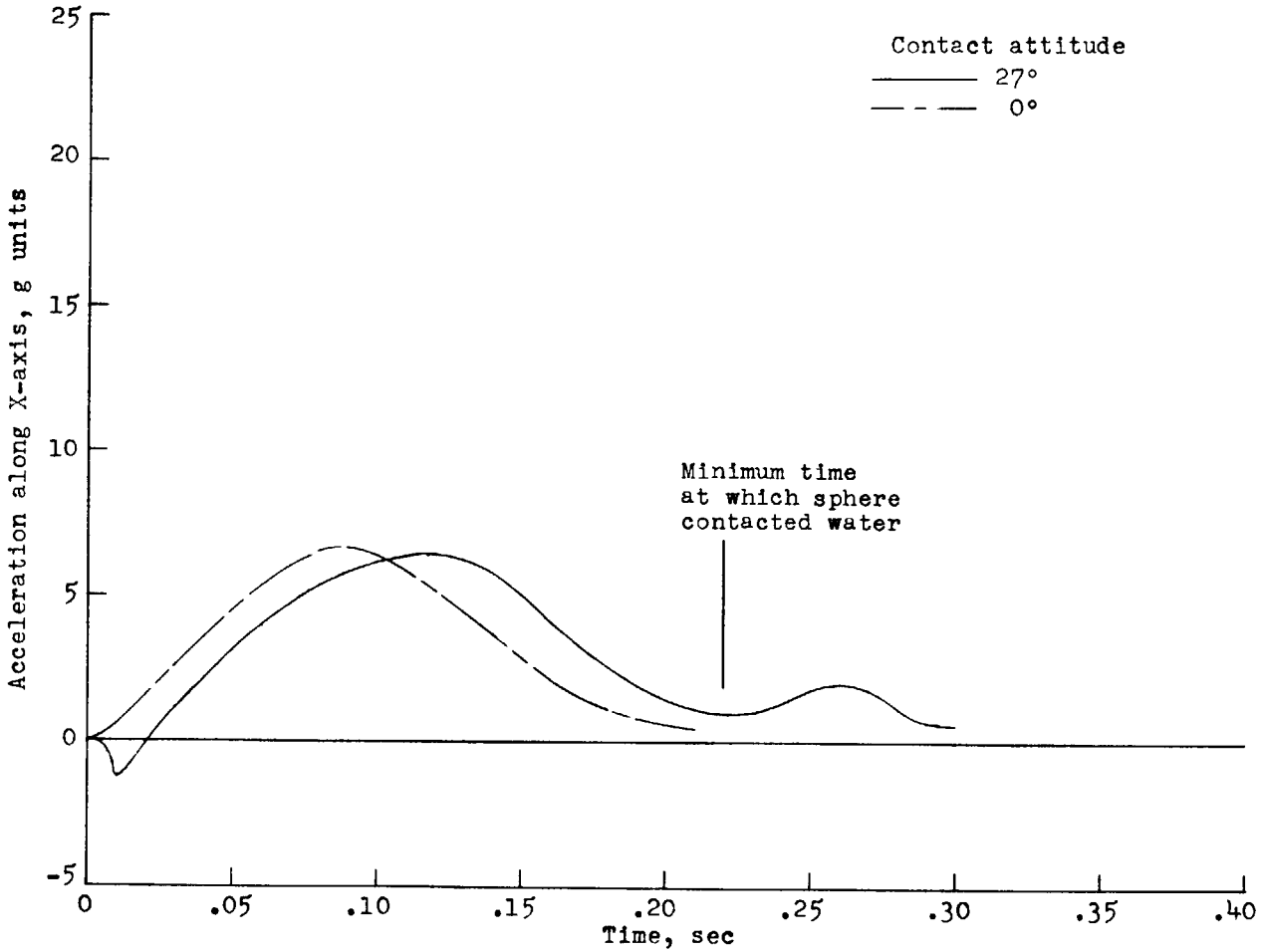

(a) Flight-path angle, 90°.

Figure 13.- Typical acceleration time histories along X-axis for landings in water. All values are full scale.

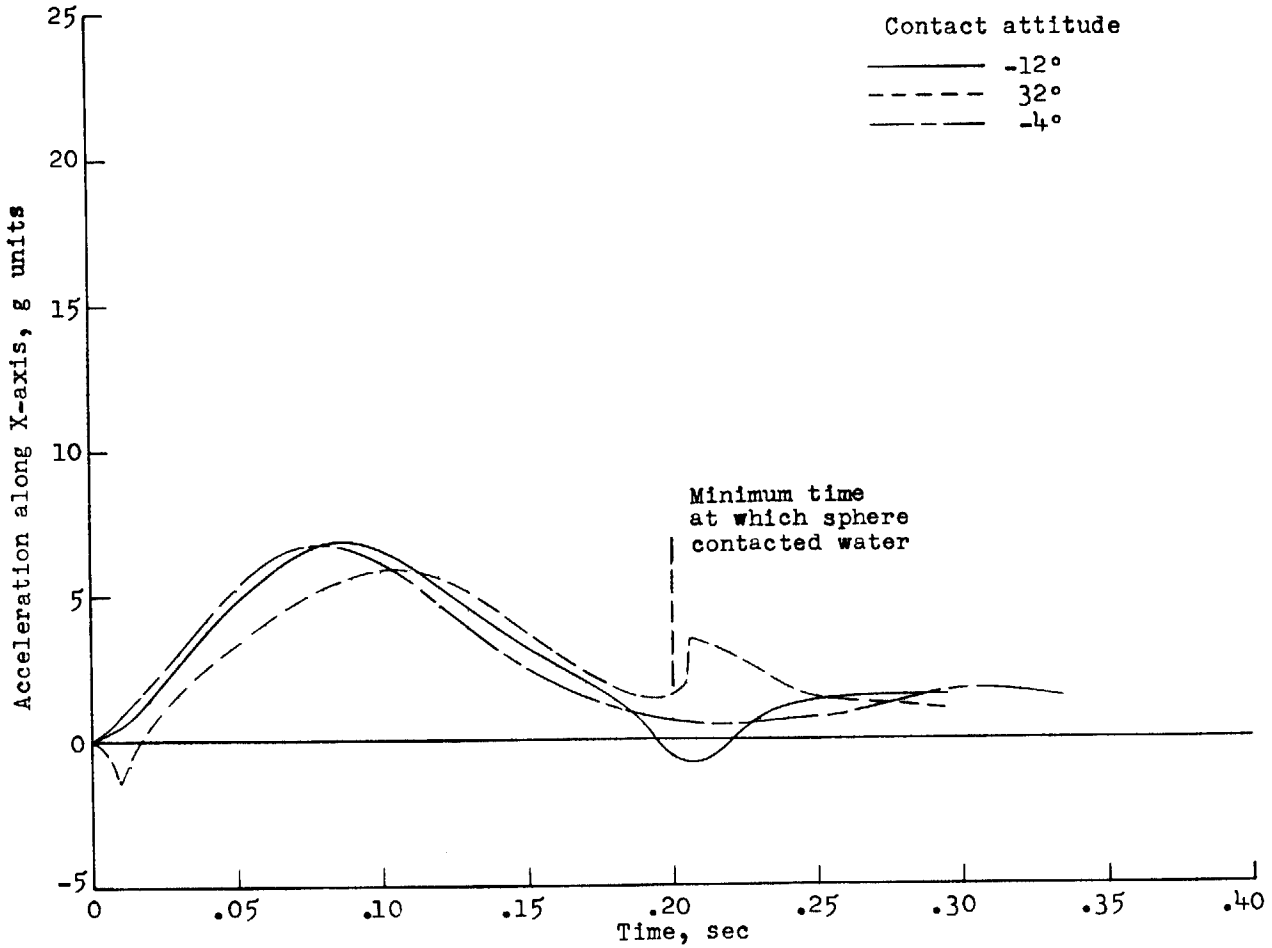

(b) Flight-path angle, 60°.

Figure 13.- Continued.

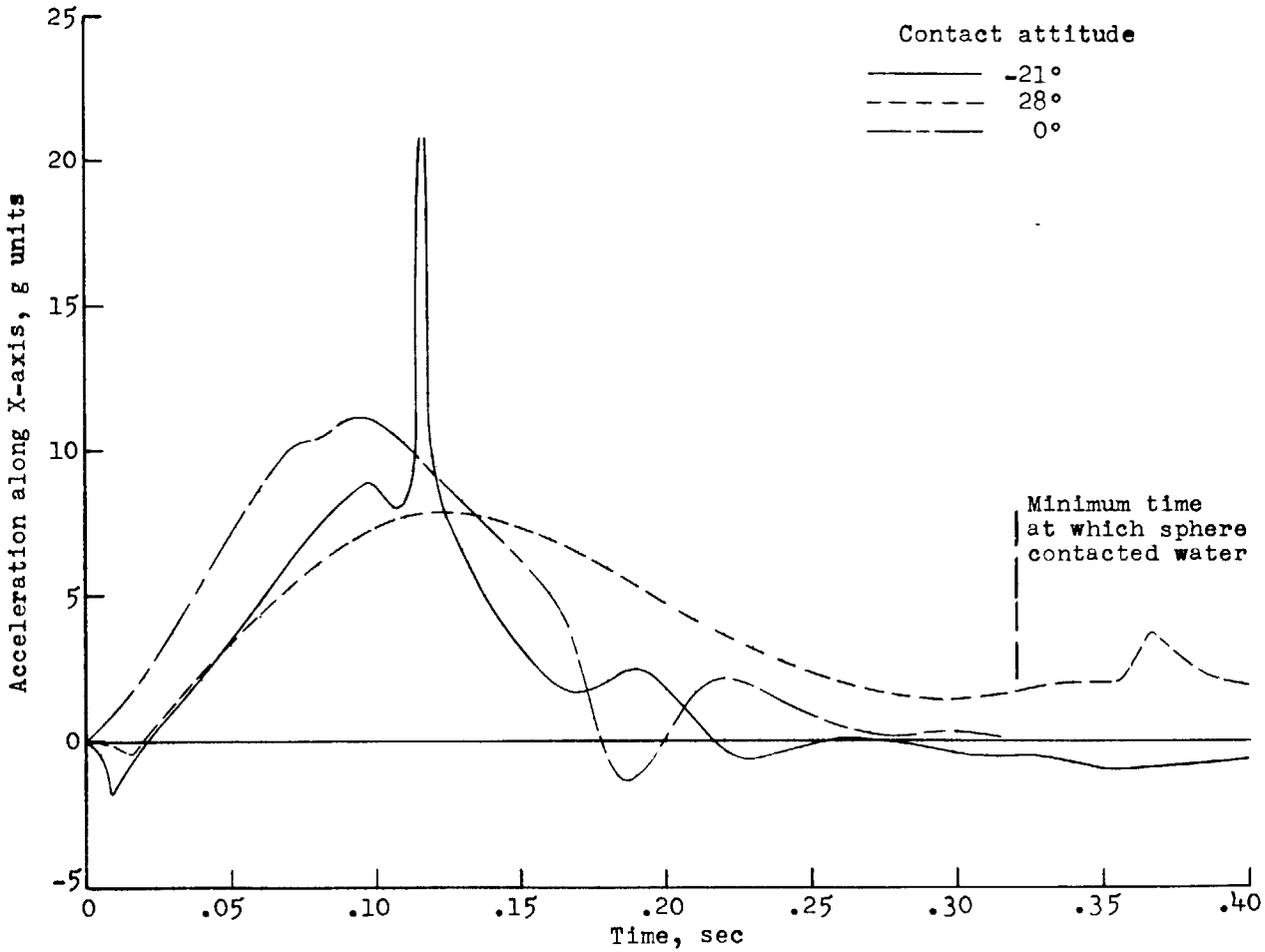

(c) Flight-path angle, 27°.

Figure 13.- Concluded.

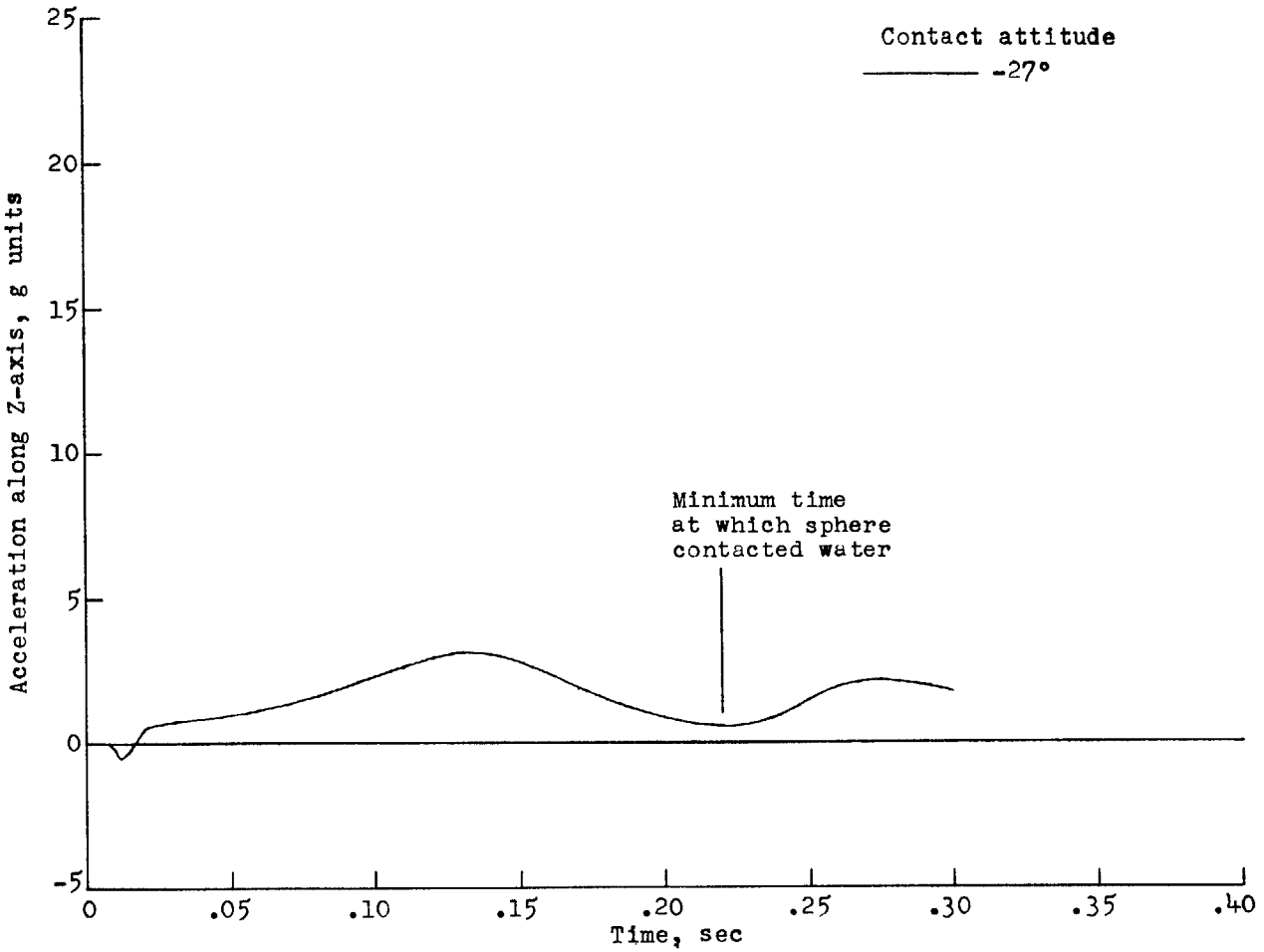

(a) Flight-path angle, 90°.

Figure 14.- Typical acceleration time histories along the Z-axis for landings in water. All values are full scale.

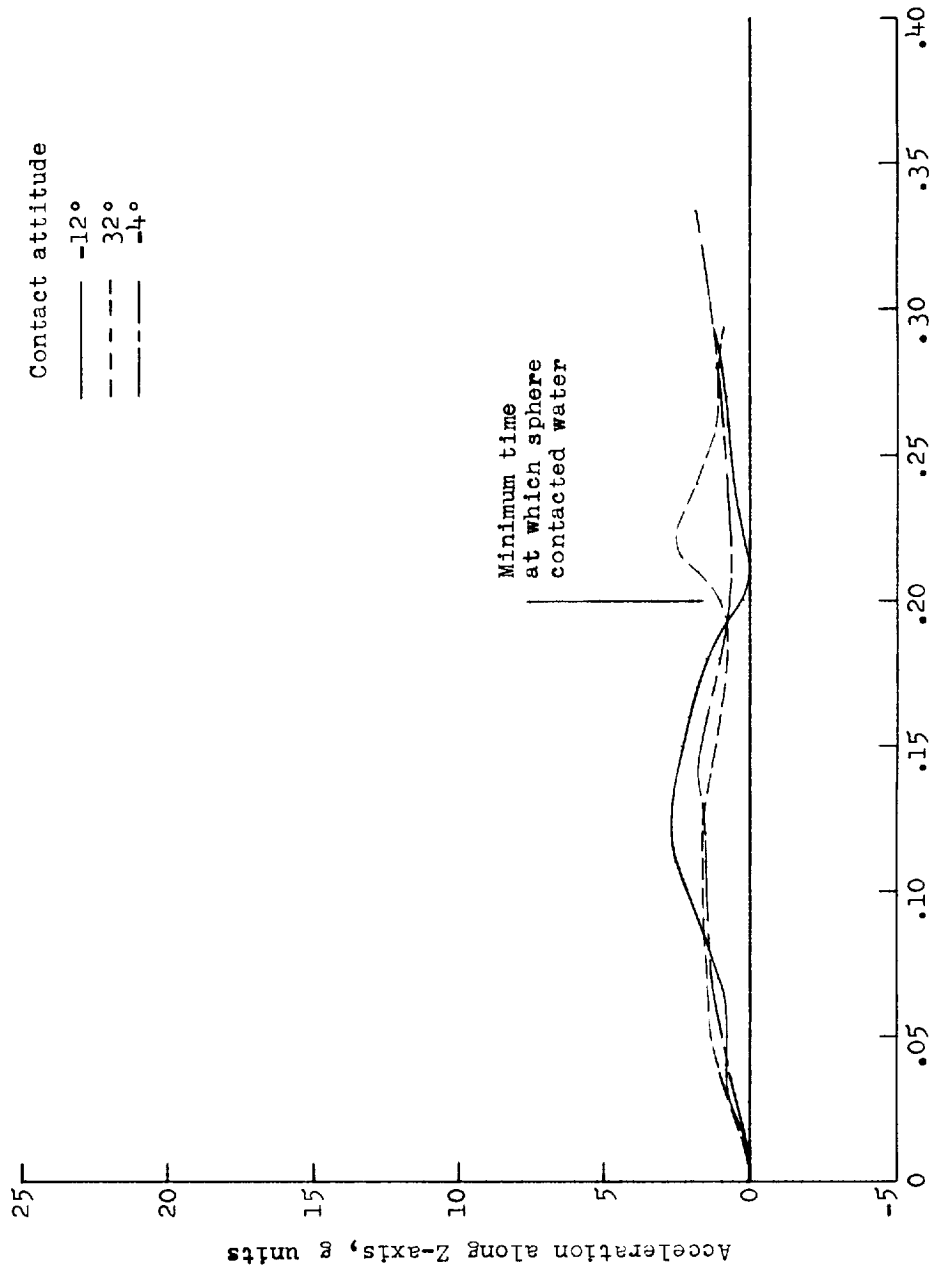

(b) Flight-path angle, 60°.

Figure 14.- Continued.

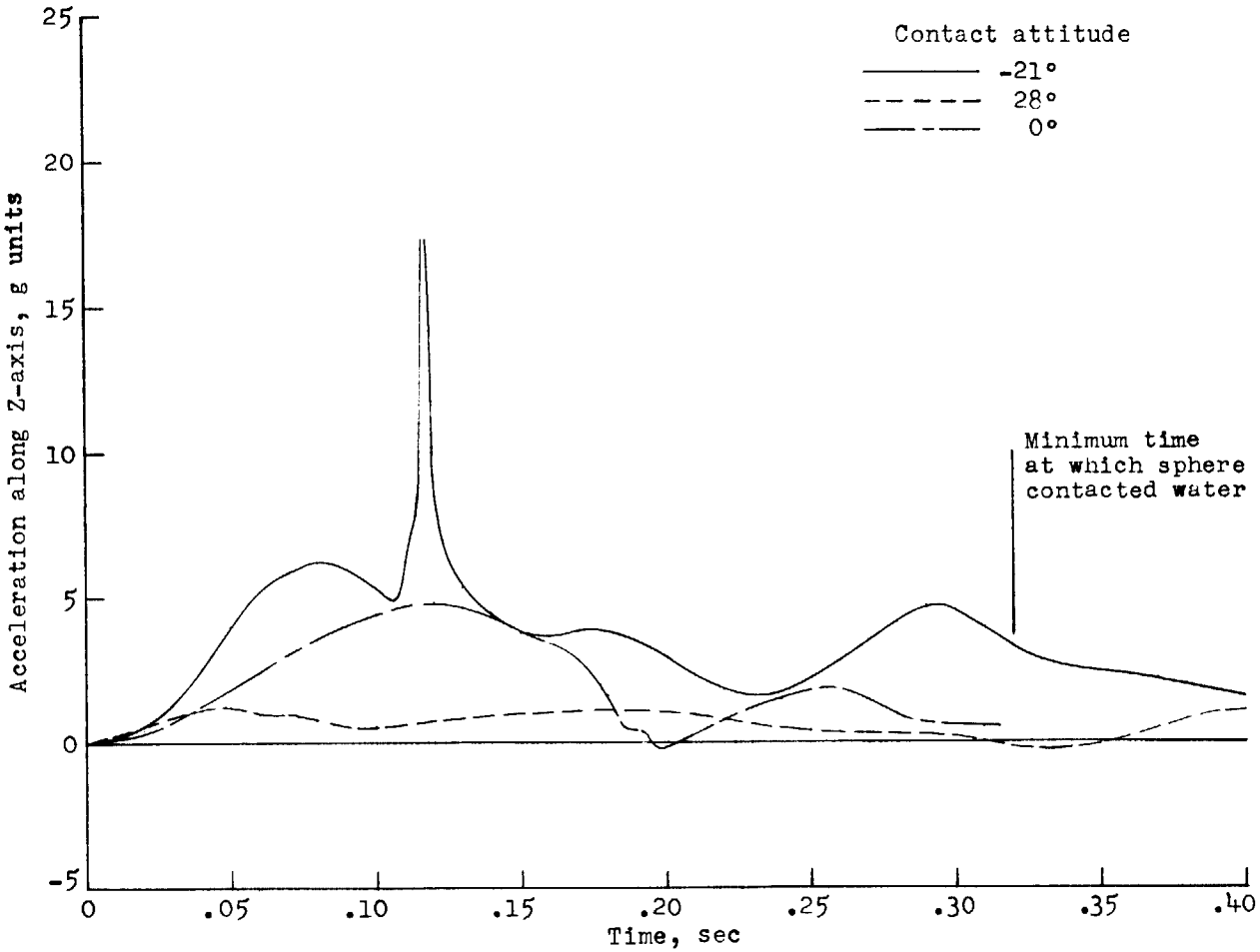

(c) Flight-path angle, 27°.

Figure 14.- Concluded.

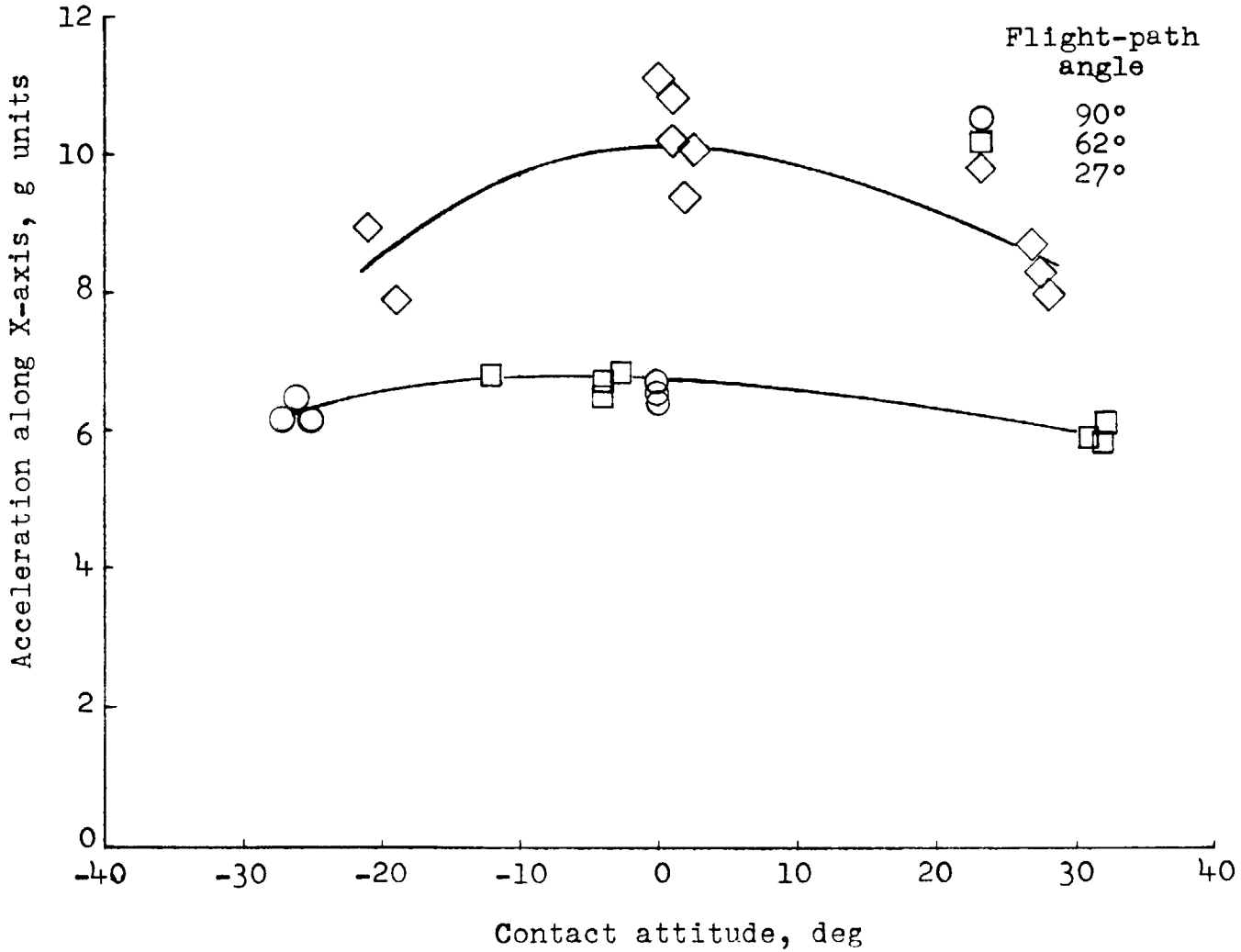

(a) X-axis.

Figure 15.- Maximum accelerations for landings in water.

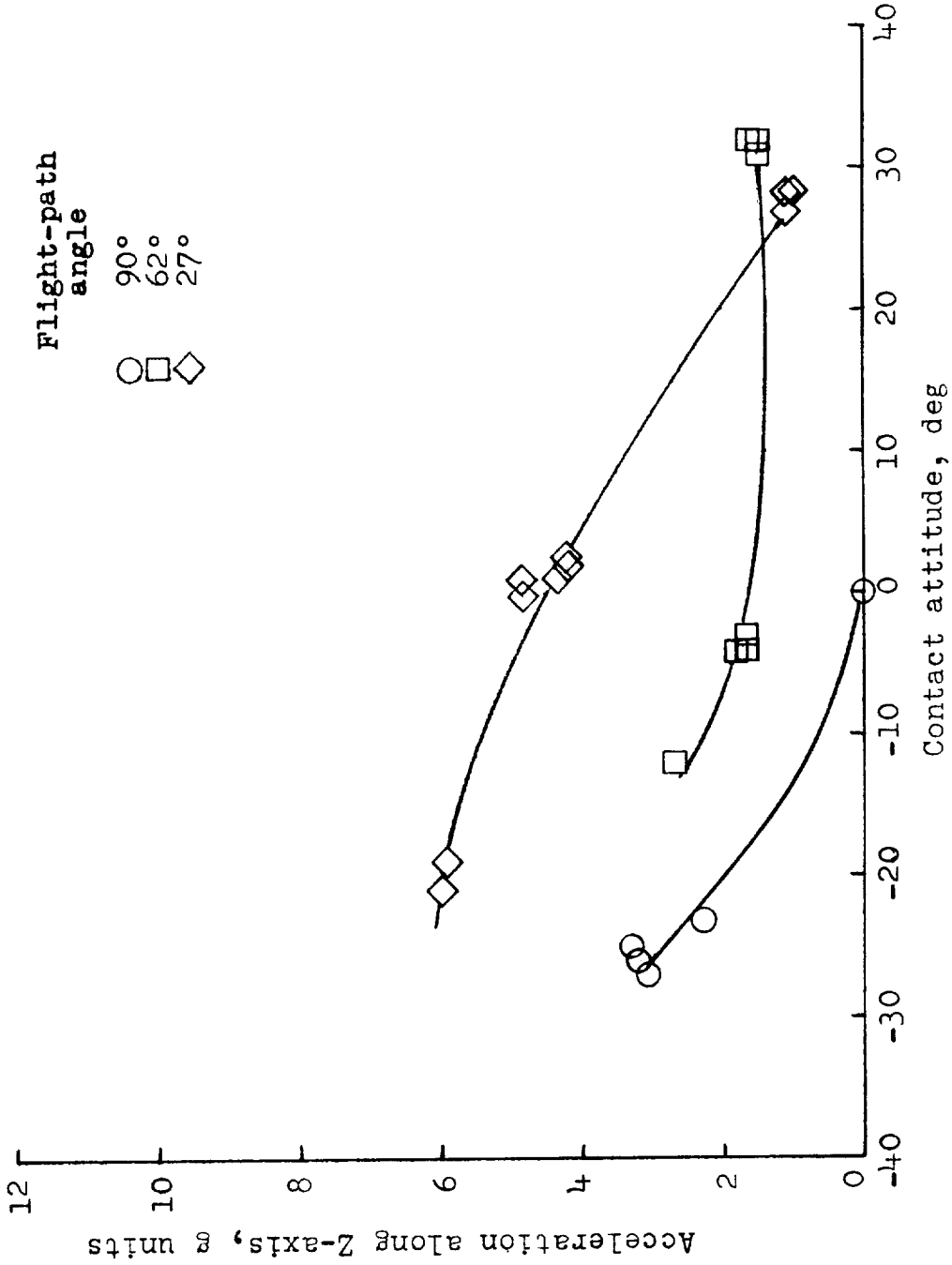

(b) Z-axis.

Figure 15.- Concluded.

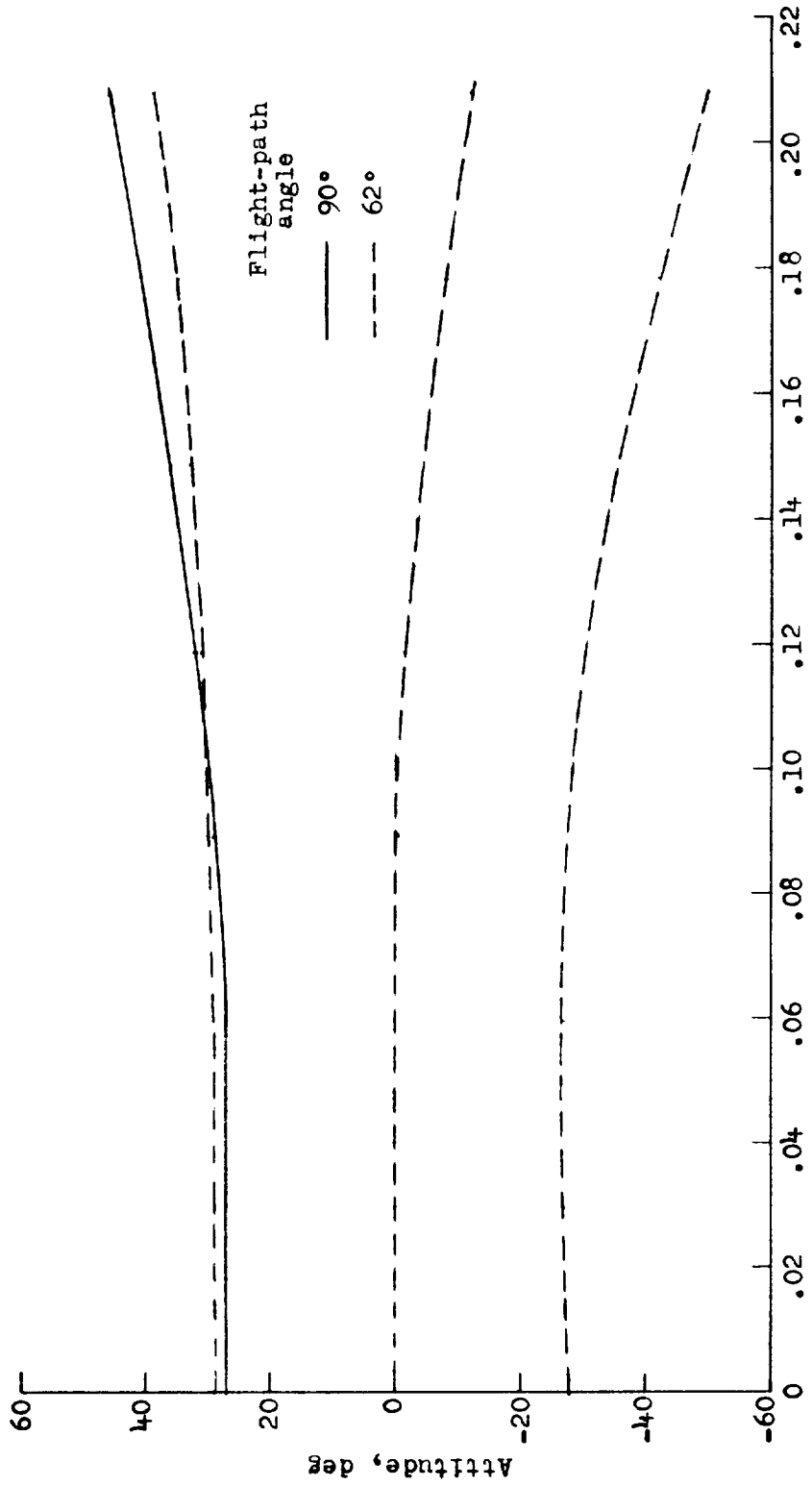

Figure 16.- Attitude time histories for landings on sand. All values are full scale.

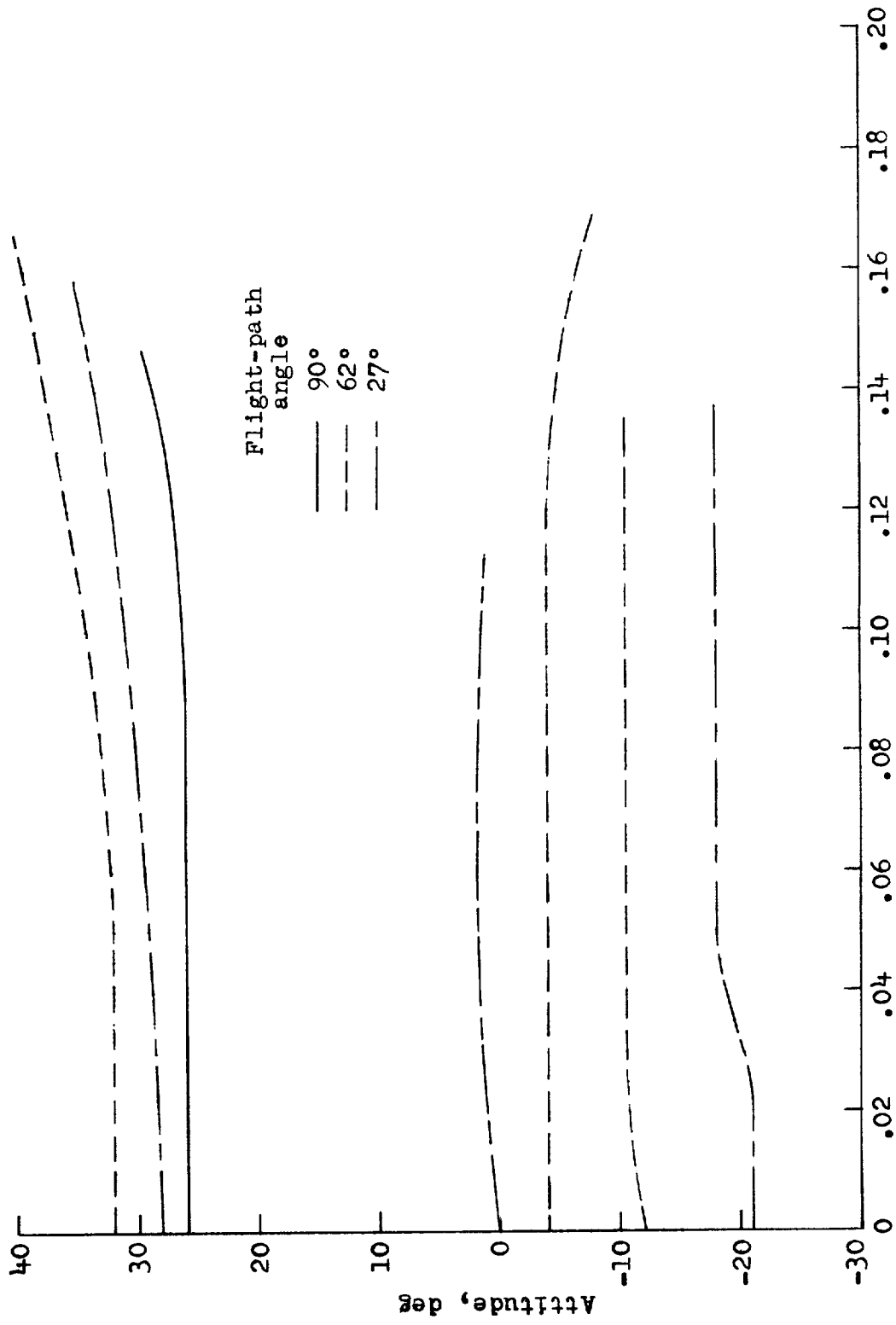

Figure 17.- Attitude time histories for landings in water. All values are full scale.

NASA-Langley, 1962 L-1319